MASTERARBEIT | MASTER'S THESIS

Titel | Title

Optimization of triple negative breast cancer spheroids

verfasst von | submitted by

Regina Assmann BSc

angestrebter akademischer Grad | in partial fulfilment of the requirements for the degree of

Magistra pharmaciae (Mag. pharm.)

Wien | Vienna, 2025

Studienkennzahl lt. Studienblatt | Degree programme code as it appears on the student record sheet:	UA 066 605
Studienrichtung lt. Studienblatt | Degree programme as it appears on the student record sheet:	Masterstudium Pharmazie
Betreut von | Supervisor:	Univ.-Prof. Dipl.-Ing. Dr. Manfred Ogris
Mitbetreut von | Co-Supervisor:	Haider Sami Ph.D.

Danksagung

Zuerst möchte ich mich hiermit recht herzlich bei Herrn Professor Manfred Ogris bedanken, dass ich meine Masterarbeit am „Laboratory of Macromolecular Cancer Therapeutics“ (MMCT)durchführen konnte.

Ich hatte das Glück während meiner praktischen Arbeit, in ein freundliches und unterstützendes Team aufgenommen worden zu sein.

Ein besonderer Dank gilt auch meinem Mitbetreuer Dr. Haider Sami für die kompetente Unterstützung und seiner positiven Art und Gelassenheit – selbst in stressigen Situationen.

Außerdem möchte ich mich bei Marlene Eder bedanken. Sie hatte immer ein offenes Ohr für mich und stand auch nach der praktischen Arbeit mit Rat und Tat zur Seite.

Vielen Dank an alle MMCT-Kolleginnen und Kollegen für die freundschaftliche Aufnahme und positive Atmosphäre sowie ganz besonders für die unterhaltsamen und aufheiternden Gespräche zwischendurch, die den Arbeitsalltag angenehmer gemacht haben.

Ein herzliches Dankeschön geht an meine Eltern, Agnes und Thomas Assmann, die mich immer unterstützt haben, und für ihre Geduld, wenn ich mal eine Prüfung nicht gleich auf Anhieb funktioniert hat oder ich mental an meine Grenzen gekommen bin. Ohne eure Unterstützung wäre ich nie so weit gekommen.

Danke auch an meine Großeltern, die sich immer alles angehört haben, was ich gerade zu lernen hatte, egal wie oft ich die Themen wiederholt habe.

Außerdem möchte ich meinen Freund Victor Ivanov danken, der mich das letzte Jahr an der Uni immer unterstützte und mir immer den Rücken gestärkt hat, wenn es mal schwer war.

Abschließend möchte ich mich noch bei meinem Bruder Markus und meinen Freunden Patricia, Alisa und Sabrina bedanken, die mich sowohl bei der Entstehung der Arbeit als auch im Laufe meines Studiums mental unterstützt haben – sei es durch motivierende Worte oder durch kurzzeitige Ablenkungen vom Alltag.

Vielen Dank!

Contents

1. ABSTRACT – ENGLISH

Since cancer is one of the most common causes of death worldwide alongside cardiovascular diseases, it is important to find new therapeutic approaches and further improve existing therapies. Breast cancer is one of the most widespread and most common types of cancer in women, which is why it deserves special attention.

This work focuses on the optimisation of 3D triple negative breast cancer (TNBC) spheroid models in order to develop more complex and suitable *in vitro* models for further research.

The Human TNBC cell line MDA-MB-231 and its lung metastasis cell line MDA-MB-231 LM2-4 were seeded in ultra-low attachment plates. Different protocols with the addition of collagen I or Geltrex® were tested to promote spheroid formation. Additionally, both cell lines were seeded together with human mammary fibroblast cell line (HMF3S) to mimic the tumour microenvironment of TNBC. Phase contract imaging, viability assays and necrotic core staining was carried out to analyse the morphology and growth of the spheroids, as well as the distribution of dead cells within.

Phase contrast photos showed that both cell lines do not form true spheroids on their own or when collagen was added. Only loose aggregates could be achieved. With the addition of Geltrex, compact spheroids could be achieved with both cell lines, which additional formed a strong necrotic core. When co-seeded with HMF3S cells, compact spheroids could be generated, resulting in a 3D models that resembles the tumour microenvironment better than monocellular spheroids.

2. ZUSAMMENFASSUNG – DEUTSCH

Da Krebs neben Herzkreislauferkrankungen zu den häufigsten Todesursachen weltweit gehört, ist es wichtig, neue Therapieansätze zu finden und bestehende Therapien weiter zu verbessern. Brustkrebs ist eine der am weitesten verbreiteten und bei Frauen am häufigsten vorkommende Krebsarten, und verdient daher besondere Aufmerksamkeit.

Diese Arbeit konzentriert sich auf die Optimierung von 3D Sphäroid-Modelle des dreifach negativen Brustkrebs (TNBC), um geeignetere und komplexere *in vitro* Modelle für weitere Forschungen zu entwickeln.

Die humane TNBC-Zelllinie MDA-MB-231 und ihre Lungenmetastasen-Zelllinie MDA-MB-231 LM2-4 wurden in „Ultra-Low-Attachment“-Platten ausgesät. Verschiedene Protokolle mit der Zugabe von Kollagen I oder Geltrex wurden getestet, um die Sphäroid-Bildung zu fördern. Zusätzlich wurden beide Zelllinien zusammen mit der humanen Mamma-Fibroblasten-Zelllinie (HMF3S) ausgesät, um die Tumormikroumgebung von TNBC nachzubilden. Phasenkontrast-Bildgebung, Viabilitätstests und nekrotische Kernfärbung wurden durchgeführt, um die Morphologie und das Wachstum der Sphäroide sowie die Verteilung abgestorbener Zellen im Inneren zu analysieren.

Phasenkontrast-Aufnahmen zeigten, dass beide Zelllinien weder allein noch unter der Zugabe von Kollagen echte Sphäroide bilden. Es konnten lediglich lose Aggregate gebildet werden. Durch die Zugabe von Geltrex konnten mit beiden Zelllinien kompakte Sphäroide erzeugt werden, die zusätzlich einen starken nekrotischen Kern bildeten. Durch die gleichzeitige Aussaat mit HMF3S-Zellen konnten kompakte Sphäroide erzeugt werden. Diese resultierenden 3D-Modellen bilden die Tumormikroumgebung besser ab als monozelluläre Sphäroide.

3. ABBREVIATION

CAFs	Cancer-associated fibroblasts
CTLA-4	cytotoxic T-lymphocyte-associated Protein 4
DAPI	4',6-Diamidin-2-phenylindol
DMEM	Dulbeccos Modified Eagle Medium
ECM	Extracellular matric
eGFP	Enhanced Ggreen Ffluorescent pProtein
ER	Estrogen receptor
FCS	Fetal calf serum
FLM	Fluorescent microscopy
H/E	Haematoxylin/eosin
HER2	Human epidermal growth factor receptor 2
HR+	Hormone receptor-positive
IHC	Immunohistochemical
LM2-4	Lung Metastatic 2 number 4
luc	Luciferase
MDA-MB-231	MD Anderson Metastatic Breast 231
PBS	Dulbecco’s phosphate buffered saline
PD-L1	Programmed Cell Death Protein 1
PFA	Paraformaldehyde
PGK	Phosphoglyceratkinase

PI	Propidium iodide
PR	Progesteron receptor
RFU	Relative fluorescence unit
RSZ	Resazurin
TAM	Tumour-associated macrophages
TME	Tumour microenvironment
TNBC	Triple negative breast cancer

4. INTRODUCTION

4.1. Breast cancer

Breast cancer is the most common malignancy and the leading cause of cancer-related death in women worldwide (1–3). It is a highly heterogeneous disease involving several tumour subtypes that differ in their morphology, gene expression profiles, clinical behaviour and response to treatment (1,2,4). This diversity is reflected in the classification of breast cancers based on the presence or absence of key biomarkers, in particular the estrogen receptor (ER), the progesterone receptor (PR) and the human epidermal growth factor receptor 2 (HER2) (1,2,5–7) . These markers are crucial for prognosis, predicting recidivism, and defining the treatment strategy.
The molecular subtypes of breast cancer – like hormone receptor-positive (HR+), HER2-positive and triple-negative breast cancer (TNBC) – result from different biological signalling pathways and have different clinical outcomes (1,2,7,8). For example, HR+ tumours generally respond better to endocrine therapies, while HER2-positive cancers benefit from specific anti-HER2 treatments. TNBC, in which all three important receptors are absent, is often more aggressive and less responsive to targeted treatments (1,2,8,9).
The clinical complexity of breast cancer is closely related to the essential characteristics of cancer. These characteristics – originally described by Hanahan and Weinberg – include the maintenance of proliferation signals, the avoidance of growth inhibitors, the resistance to cell death, enabling replicative immortality, the induction of angiogenesis, the initiation of invasion and metastasis, the alteration of cellular metabolism and resistance to immune destruction, all supported by enabling characteristics such as genomic instability and cancer-promoting inflammation, which together facilitate the acquisition of these hallmark capabilities (1,2,10–12). In breast cancer, certain characteristics are particularly prominent depending on the molecular subtype. For example, the preservation of proliferative signalling is essential for hormone receptor-positive tumours, while invasion, metastasis, and immune evasion are particularly relevant in triple-negative breast cancers. The interaction of these characteristics not only promotes tumour development and progression, but also reinforces the ongoing challenges in the diagnosis, classification and treatment of breast cancer. As research moves forward, a deeper understanding of how these features show up in different subtypes of breast cancer keeps bringing insights for developing more accurate and effective therapies (7).

4.1.1. Environmental challenges

Environmental factors play a complex and increasing well-recognised role in the development of breast cancer. Among these, exposure to ionising radiation is the best-documented environmental risk factor, with the risk being highest when exposure occurs at a young age. Even low-dose medical radiation, as found in CT scans and

mammograms, has been shown to increase the risk of breast cancer and is believed to be responsible for an estimated 1 % of cases (13). Air pollution, in particular higher concentrations of nitrogen dioxide (NO_2), a traffic-related substance, is also associated with an elevated risk of breast cancer (14,15) . In addition, chronic exposure to overall low environmental quality—including soil contamination, air and water pollution, and the urban environment—is related to higher breast cancer rates, especially in places like cities. In such regions, studies have observed an average increase of about 10.8 additional breast cancer cases per 100 000 people compared to areas with better environmental quality (16).

The possible effects of chemicals in the environment are currently being investigated, specifically those with estrogen-like properties, such as certain pesticides, polychlorinated biphenyls (PCBs) and chemicals found in plastics and body care products (17). Although the clear connection between these chemicals and breast cancer risk is still unclear at this point in human studies, the ability of these chemicals to mimic hormones raises concerns about their potential role in tumour development (18). Other environmental influences that have been studied are tobacco smoke, with some evidence indicating that long-term heavy smoking may be associated with a slight increase in breast cancer risk, especially if smoking begins before a woman's first pregnancy. But the evidence for both direct and passive smoking remains suggestive but inconclusive (19). Lifestyle-related environmental factors such as alcohol consumption (20), lack of exercise and exposure to light at night (e.g. due to shift work) (21) have also been associated with an elevated risk of breast cancer, although the mechanisms and degree of these effects are still being investigated (22,23).

Overall, certain environmental influences are clearly associated with breast cancer, while others are still the subject of ongoing research. The time of exposure, genetic predisposition and the cumulative effect of several environmental factors add to the complexity of breast cancer risk evaluation(16,22).

4.1.2. Breast cancer microenvironment

The tumour microenvironment (TME) of breast cancer has unique pathophysiological characteristics that promote tumour initiation, progression and metastasis due to complex interactions between malignant cells and stromal elements (24). This dynamic ecosystem includes immune cells, adipocytes, endothelial cells, cancer-associated fibroblasts (CAFs) and the extracellular matrix (ECM), which together create an immunosuppressive, tumour-promoting niche (25–27). Key mechanisms include immune evasion, hypoxia-induced adaptations, and ECM remodeling, all of which contribute to therapy resistance and aggressive phenotypes (24,25,27).

Components and dynamics of the breast cancer microenvironment

The TME is subject to significant changes during the progression of breast cancer:

- *Transition from in situ to invasive carcinoma:* The destruction of the basement membrane and the loss of myoepithelial cells allow tumour cells to invade the

surrounding stromal tissue (24,28). This process includes increased secreted proteolytic enzymes (e.g., matrix metalloproteinases) by tumours and stromal cells, which makes it easier to destroy the ECM and spread locally (27–29).

- *Recruiting immuno- and stromal cells:* Tumour cells recruit tumour-associated macrophages (TAMs), CAFs and lymphocytes, thereby creating a cytokine-rich environment which promotes proliferation and metastasis (24–26). CAFs, the dominant stromal cell type, secrete growth factors and ECM-modifying proteins that enhance tumour aggressiveness .
- *Hypoxia and acidosis:* Hypoxia develops in areas with poor blood supply, inducing aggressive phenotypes (e.g. estrogen receptor negative) and metastatic spread (24,27). In addition, acidic conditions increase invasion by modifying the ECM architecture and interfering with the uptake of chemotherapeutic agents (24,27).

Role in tumour progression and immune evasion

Breast cancer utilises specific mechanisms to suppress anti-tumour immunity:

- *Expression of immune checkpoints:* Tumour cells overexpress CTLA-4 and PD-L1 to suppress cytotoxic T cell activity, creating an immunosuppressive milieu (25,26).
- *Unique evasion pathways:* TNBC uses the Lgals2-CSF1-CSF1R pathway to avoid immune detection while mimicking anti-inflammatory neuronal mechanisms (25,30,31).
- *Stromal immunosuppression:* M2-polarised TAMs and regulatory T cells dominate the TNBC microenvironment, correlate with poor prognosis(27,31,32). These cells secrete IL-10 and TGF-β, suppressing effective immune responses (26,31,32).

Implications for therapy and prognosis

The tumour microenvironment affects response to treatment and disease progression:

- *Biomarker potential:* Stromal cell compositional characteristics (e.g., tumour infiltrating lymphocytes density in TNBC) can predict response to therapy and survival . Hypoxia markers are linked to radiation resistance (27).
- *Therapeutic targets:* The strategies include interrupting the communication between CAF and tumour, the repolarisation of TAMs and the combining of immune checkpoint inhibitors with microenvironment modulators (e.g. VEGF inhibitors) (26,27,30,33). Synergistic approaches like JAK inhibitors (Ruxolitinib) with Calcitriol are showing promise in TNBC models (33).
- *Metastatic niche:* Circulating tumour cells use VEGF-C to interact with endothelial cells, which helps lymphangiogenesis and distant metastasis (27).

In summary, the microenvironment of breast cancer represents a key pathophysiological interface where stroma-tumour interactions mediate disease

progression, immune escape, and therapeutic resistance. Therapeutically targeting its unique characteristics opens new avenues for precision oncology (24).

4.1.3. Triple negative breast cancer

TNBC is an aggressive subtype of breast cancer characterized by the absence of ER, PR, and HER2 expression. TNBC makes up about 15–20 % of all breast cancer cases and is associated with a higher risk of distant metastases and poorer clinical outcomes compared to other breast cancer subtypes (8,34). With all the different places TNBC can spread to, the lungs are one of the most common and medically important for metastases (34–37). Patients with TNBC are more likely to develop lung metastases than patients with other types of breast cancer, and lung metastases are linked to a particularly poor prognosis (34,37). Studies show the median survival time for TNBC patients with lung metastases is about 18 months, which is significantly shorter than the survival time for metastases in other organs like bones or liver . The chance of getting TNBC lung metastases is affected by age, tumour size, and stage at diagnosis (35,37). Biologically, TNBC tumours that metastasise to the lungs have some unique features. Research has shown that lung metastases from TNBC are diverse, with a more varied population of cancer cells than metastases in other organs like liver (37). This difference might be part of why lung metastases are often more aggressive and difficult to treat. In addition, the microenvironment of the lung itself seems to play an important role in the growth of metastatic TNBC cells. For example, lung-derived selectins – cell adhesion molecules – can increase the migration and metastatic behaviour of TNBC cells, indicating that interactions between tumour cells and lung specific factors are important for the development and progression of metastases (36,37).
Recent studies also identified metabolic changes in TNBC cells that end up in the lungs. These cancer cells often upregulate genes involved with fatty acid metabolism, boosting their energy production and supporting their rapid growth in the lung environment (39). This type of metabolic reprogramming could lead to new ways for targeted therapy (39). In summary, TNBC shows a strong tendency to metastasise to the lungs, where the results are biologically diverse and metabolically adaptable tumours that are linked to poor survival rates. The unique interacting between TNBC cells and the lung microenvironment continues to be an important focus of research, which aims to improve prognosis and develop more effective treatments for these challenging forms of breast cancer (8).

4.1.3.1. MDA-MB-231

The MDA-MB-231 cell line is one of the most common *in vitro* models used to study TNBC (40). MDA-MB-231 cells were collected in 1976 from the pleural effusion of a 51-year-old woman with metastatic breast cancer and are known for not having ER, PR, or HER2 expression, calling them ‘triple negative’ (40–42). This receptor profile is linked to resistance to hormone therapies and HER2-targeted treatments, highlighting the clinical challenges of TNBC (40,41).

Morphologically, MDA-MB-231 cells appear epithelial-like, somewhat fusiform in appearance, and show features of epithelial-mesenchymal transition (EMT), a process that is associated with increased invasion and metastatic potential (40,41,43). The cells are both highly migratory and invasive in the two-dimensional (2D) and three-dimensional (3D) culture systems and, when implanted in animal models, tend to metastasise, making their use valuable for studying the mechanisms behind cancer cell invasion and spreading (40,41,44). At the molecular level, MDA-MB-231 cells are E-cadherin-negative, overexpress mutant p53, and have high levels of mesenchymal markers like vimentin and the stem cell surface marker profile CD44+/CD24low/–, that is present in over 90 % of the population (40,43). This phenotypic profile is associated with low differentiation and aggressive tumour behaviour (40,43).
Recently, studies using 3D spheroid cultures have shown that MDA-MB-231 cells maintain their viability and exhibit zoning characteristics in this configuration and even greater resistance to chemotherapeutic agents than in standard 2D cultures (40,41,43). The spheroids also express increased EMT markers and migratory ability, providing a promising preclinical model for studying breast cancer progression and drug resistance (40,41,43).
While MDA-MB-231 is characterised as a basal-like, triple-negative cell line, genomic analyses showed that their profile differs a lot from primary basal-like metastatic breast cancer in patients, which highlights the important role of choosing the right model for translation research (43). Still, MDA-MB-231 cells remain an important part of breast cancer research because of its aggressive phenotype, its stem cell-like properties, and its high potential for metastasis, specifically for studying the biology and therapeutic targets of triple-negative disease (40,41,43).

4.1.3.2. LM2-4

The LM2-4 cell line is a high-metastatic variant that was derived from the parental triple-negative human breast cancer cell line MDA-MB-231. It was obtained through multiple rounds of *in vivo* selection in mice. Because of its ability to metastasise to the lungs, it is considered to be a lung-selective metastatic derivative (42,45,46). LM2-4 cells maintain the triple-negative phenotype – lacking ER, PR and HER2 expression – characterised by aggressive breast cancers with limited treatment options (42,45).
Functionally, the LM2-4 cells are known for their increased potential to cause metastasis compared to the initial MDA-MB-231 cells (42,47). They are often used in preclinical research, to model the spontaneous metastasis process, specifically to the lungs, to investigate the mechanisms that drive metastasis in triple-negative breast cancer (42,45,47). Animal models show that LM2-4 cells develop lung metastasis quickly and robustly once the primary tumour is removed, which mirrors the aggressive behaviour of the disease in humans (42,47). Additionally, a rapid onset of tumour growth could be observed when implanted orthotopically in SCID mice, where tumours reached a size > 500 mm^3 within three weeks. In contrast, the original cell line MDA-MB-231 grows slowly over months in the same animal model. (48). Research has shown that

LM2-4 cells need certain pathways to grow and survive. The sphingosine kinase (SphK) and sphingosine-1-phosphate (S1P) signalling pathways are critical for the proliferation and survival of LM2-4 cells, since inhibition of these pathways significantly affects their viability, a phenomenon not found in the original MDA-MB-231 cell line (45). These findings highlight the unique biology of LM2-4 cells and the value of this model for investigating lung-specific metastasis, tumour progression, as well as drug resistance in triple-negative breast cancer (45).

4.2. 2D cell culture vs. 3D cell culture

2D cell cultures are a fundamental tool in biomedical research, specifically in cancer biology. In these cultures, cells grow as a single layer on flat, solid plastic surfaces, such as the bottom of culture plates or flasks. This approach offers multiple advantages: it has low technical complexity, is inexpensive, and allows simple observation, manipulation, and analyzation of cell behaviour (49,50). For these reasons, 2D-cell cultures have become the standard model for *in vitro* experiments, such as drug screening, mechanistic studies, and genetic manipulations (49,50). Despite being widely used, 2D cell cultivation has some serious limitations. This flat, two-dimensional setting can't replicate the complex three-dimensional architecture, cell-cell interactions, or microenvironment gradients that are present in living tissues and tumours (50,51) . This lack of physiological relevancy can result in inconsistencies between experimental *in vitro* results and *in vivo* or clinical settings. As an example, cancer cells grown in 2D commonly exhibit altered morphology, gene expression, and drug sensitivity compared to cells in 3D cultures or actual tumours (50–52).
These limitations are particularly obvious in drug development: many drug candidates that appear promising in 2D cell culture models fail in animal testing or clinical trials, partly due to the fact that 2D cultures do not precisely mimic the tumour microenvironment and the lack of physical barriers to drug penetration found in real tumours (50,51) . Therefore, while 2D cell cultures remain essential for basic research and high-throughput screening, there is an increasing focus on the development and application of more physiologically relevant 3D culture systems to narrow the gap between *in vitro* studies and the clinical reality(51) (50,51). The 3D cell culture is a significant improvement over traditional 2D culture systems, particularly in cancer research. In 3D cultures, the cells are grown in an environment that mimics the architecture, complexity, and microenvironment of real tissues and tumours better. This can also be achieved by various methods, including scaffold-based systems, hydrogels and, most commonly, the creation of spheroids – dense, spherical cell aggregates that self-organise and are interactive in all three dimensions (49–51).

4.2.1. Spheroids

Spheroids are three-dimensional cell clusters that form naturally in culture environments in which cell-cell and cell-extracellular matrix (ECM) interactions are prioritised over cell-substrate adhesion (53–55). These structures mimic the architecture, microenvironment, and functional properties of avascular tumour sites, which makes them highly relevant models for investigating cancer biology and drug responses.

Formation and structure

Initially, individual cells assemble into loose clusters, a process that is mediated by long-chain ECM fibres binding to integrins on the cell membrane.
This aggregation induces high cadherin expression, causing cadherins to accumulate at the cell membrane.
Homophilic cadherin-cadherin bonding is then used to pack the cells into solid, stable spheroids(53).
The nature and concentration of ECM fibres and cadherins are different depending on the cell type. For example, E-cadherin is important for the tight packing in some breast cancer cell lines, whereas other lines like MDA-MB-231 form spheres mostly through collagen I/integrin β interactions instead of cadherin (53). Additional adhesive proteins, such as connexins and pannexins, and the remodelling of the cytoskeleton (especially actin filaments) are also involved in spheroid formation and stability (53).

Physiological zoning

Spheroids typically have a layered structure:

- An external proliferative zone, in which the cells are highly active and have access to nutrients and oxygen.
- A middle resting zone, in whom the limited diffusion of nutrients and growth factors leads to the cells to slow down their proliferation.
- An internal necrotic core, especially in bigger spheroids, caused by hypoxia and nutrient deficiency (54,56).

These zones reflect *in vivo* gradients found in solid tumours, like oxygen and nutrient gradients, waste accumulation, and changes in pH, causing changes in gene expression and metabolic adaptation (e.g., the Warburg effect in hypoxic centres) (54).

Biological and research relevance

Spheroids replicate many *in vivo* tumour characteristics:

- Dynamic cell-cell and cell-ECM interactions
- Gradients of nutrients, oxygen and signalling molecules
- Different proliferation, resting and necrosis zones
- More physiologically relevant gene expression and signal transduction compared to 2D cultures (53,54,56)

These properties make spheroids useful for studying tumour growth, invasion, metastasis, and drug resistance. They are also used for studying the tumour microenvironment, including the interactions between cancer cells and stromal or immune cells, as well as for testing the efficacy and penetrability of cancer drugs in an setting that better reflects *in vivo* responses (53,54).
In summary, spheroids are a robust and physiologically relevant 3D culture model, bridging the gap between simple cell monolayers and complex animal models and allowing deeper insights in tumour biology and the response to therapies (53,54).

4.2.2. Multicellular spheroids

Spheroids containing both cancer cells and fibroblasts are an advanced 3D co-culture model that replicate the tumour microenvironment more accurately than monocultures of cancer cells. Fibroblasts, especially CAFs, the most common stromal cell type in breast tumours, take on a dynamic role in tumour progression, invasion, and therapy resistance (57,58).

Formation and structure
Cancer cells and fibroblasts are mixed in these co-culture spheroids, allowing direct cell-cell contact and complex paracrine signalling. The fibroblasts can be either normal fibroblasts or CAFs, the last ones having a phenotype that actively supports tumour growth (58). The inclusion of fibroblasts results in the formation of a more physiologically relevant ECM, including compounds such as fibronectin and collagen, further supporting tumour-like structure and behaviour (58).

Biological interactions and impacts
Fibroblasts in spheroids secrete chemokines like CXCL12, that interact with receptors like CXCR4 on TNBC cells, boosting their proliferation and metabolism a lot (57,59). This chemokine signal axis is also involved in promoting the invasive behaviour of cancer cells in the surrounding matrix, as seen when spheroids are embedded in collagen gels (59). The activity of oncogenic pathways, like MAPK/ERK and PI3K/AKT, is higher in these co-cultures, which makes them more resistant to chemo drugs like paclitaxel (57).

Specific reactions for each subtype
The impact of fibroblasts on the way cancer cells act in spheroids is specific to the subtype. Basal breast cancer cells (including TNBC) show increased motility and invasive behaviour in co-cultures with fibroblasts, whereas luminal cells tend to keep a non-invasive, benign structure even when fibroblasts are present (60). This indicates that the microenvironmental signalling provided by fibroblasts is particularly effective in promoting invasion in aggressive breast cancer subtypes.

Therapeutic implications

The interaction between cancer cells and fibroblasts in spheroids could make cancer cells more resistant to therapy, which highlights the importance of targeting not just the cancer cells, but also their supporting stroma components and signalling pathways (57,61,62). Disrupting important signalling axes such as CXCL12–CXCR4 or blocking activated pathways such as MAPK/ERK and PI3K/AKT can lower the proliferation and survivability of cancer cells in these models (57).

Summary

Cancer fibroblast spheroids provide a robust platform for studying tumour-stromal interactions, invasion, drug resistance and the molecular mechanics behind cancer progression. These models are essential for preclinical testing of therapeutics that target both cancer cells and their microenvironment, offering insights into *in vivo* tumour behaviour that are more accurate than those provided by conventional monoculture systems (57,58,60).

4.2.2.1. HMF3S

The HMF3S cell line contains immortalised human breast fibroblasts that were taken from healthy breast tissue. This cell line is frequently used in breast cancer research as an appropriate model for the breast stroma environment (63–65). It plays a critical role in studies investigating the interactions between fibroblasts and breast cancer cells, especially in relation to tumour growth and invasion (63,64). Interestingly, when co-cultured or co-injected with breast cancer cells, HMF3S fibroblasts enhance cancer cell invasion, tumour growth, and stroma activation, partially through increased cytokine secretion and remodelling of extracellular matrix proteins (64). Their sensitivity to factors such as TGF-β1 also makes them valuable for researching the mechanisms behind the activation of cancer-associated fibroblasts (CAFs) (63,65).

5. AIM OF MASTER THESIS

The main aim of this thesis was to optimize the generation of monocellular spheroids of TNBC cell lines MDA-MB-231 PGK eGFP luc and MDA-MB-231 LM2-4 eGFP luc and multicellular spheroids together with human breast fibroblasts HMF3S.

The first goal of the work was to produce monocellular spheroids from the above-mentioned cell lines. To this end, different collagen concentrations were initially used, followed by additional centrifugation. Cell growth and behaviour were examined using phase contrast photos and resazurin assays. Hoechst/PI staining was also performed to identify and observe the necrotic nucleus and dead cells in the cell aggregates. Later, Geltrex was used as a substitute for collagen to see how growth and spheroid formation changed at different concentrations.

The second objective of the work was to produce multicellular spheroids in co-culture from breast cancer cells by adding the human mammary fibroblast cell line HMF3S to create an *in vitro* breast cancer model similar to the *in vivo* pathophysiology. Similarly, spheroid formation and growth was documented on a daily basis using phase contrast photos and viability assays. Live-dead staining was performed again to document cell death and to enable comparison of the different models.

6. MATERIAL

6.1. Materials

All used Materials are shown in Table 1 below.

Table 1: List of used materials, including manufacturer and Reference-numbers

Materials	Manufactorer	Reference-Numbers
COSTAR ® ultra-low attachment 96-well plate, round bottom	Corning Incorporated	Ref.: 7007
CELLSTAR 96-well, cell culture-treated, F-bottom microplate (white)	Greiner BioOne	Ref: 655098
Nunclon delta surface, flat 96 well plate	ThermoScientific	Ref.: 167008
CT15 tubes	Sarstedt	Ref.: 62.554.502
CT50 tubes	Sarstedt	Ref.: 62.548.004
Cell culture T75 flask	Sarstedt	Ref.: 83.3911.002
Small tubes (0.5, 1.5, 2.0mL)	Eppendorf	
Serological Pipettes, 5mL	Sarstedt	Ref.: 86.1253.001
Serological Pipettes, 10mL	Sarstedt	Ref.: 86.1254.001
Serological Pipettes, 25mL	Sarstedt	Ref.: 86.1685.001
Pipette boy	VWR International	
Pipette tips (10, 200, 300, 1000 µL)	Nerbe plus GmbH/ Eppendorf	
Pipette (2.5, 10, 100, 200, 1000 µL)	Eppendorf and/or Sarstedt	
Syringe filter, PES 0.2µL	fisherbrand	Ref.: 15206869
Inject Luer Solo, 10mL	Braun	Ref.: 4606108V
Coverslips, 24x50mm	Epredia / Carl Roth	Ref.: BB02400500A113MNZ0
Superfrost Microscope Slides	Epredia	Ref.: AA00008032E01MNZ10
Superfrost Plus Adhesion Microscope Slides	Epredia	Ref.: J1800AMNZ
Tissue tek O.C.T. Compund	Sakura	Ref.: 4583
Disposable base mold	EMS	Ref.: 62352-07

6.2. Cell lines

The used cell lines are shown in Table 2 below.

Table 2: List of used cell lines, including manufacturer

Cells	**Manufacturer**
LM2-4 eGFP luc	MMCT
MDA-MB-231 PGK eGFP luc	MMCT
HMF3S	Ludwig Institute for Cancer Research Ltd

Both TNBC cell lines MDA-MB-231/LM2-4 were transduced with a lentiviral vector encoding for PGK-eGFP luc. After the transduction, cells were fluorescently sorted to obtain only eGFP luc positive cells for further cultivation (48,66) .

6.3. Medium

The used Media is shown in Table 3 below.

Table 3: List of used Media, including Manufacturer, reference- and LOT-number

Material	**Manufacturer**	**Reference- and LOT-Number**
DMEM high glucose	Sigma-Aldrich	Ref.: D5671 LOT.: RNBM4850

6.4. Liquids and powders

The used liquids and powders are shown in Table 4 below.

Table 4: List of used liquids and powders, including Manufacturer and Reference number or LOT-number

Material	**Manufacturer**	**Reference- / LOT-Number**
Fetal calf serum (FCS), heat inactivated	BioWest	Ref.:
Penicillin-Streptomycin	Sigma	Ref.: P0781
L-Glutamine 200mM solution	Sigma	Ref.: G7513
TrypLE Express enzyme w/o phenolred	Gibco	Ref.: 12604021
Dulbecco´s Phosphate Buffered Saline Modified (PBS)	Sigma-Aldrich	Ref.: D8537 LOT: RNBM5276
Resazurine powder, sodium salt, pure	ThermoScientific	Ref.: 418900050 LOT: A0464132

Hoechst (10mg/mL)	Sigma-Aldrich	Ref.: 33342
Propidium iodide (1,0mg/mL)	Sigma-Aldrich	CAS.: 25535-16-4
Collagen from calf skin	Sigma-Aldrich	LOT: SLCD5043
Geltrex	Gibco	Ref.: A14132-01 LOT: 1008585A
PFA 4% in HBS pH 7,4	BioChemica	LOT: 4V008654 PanReac LOT: 7E011523 PanReac
Triton-X-100: Laboratory grade	Sigma-Aldrich	LOT: SLBM3864V
DAPI Staining Solution (1mg/mL)	Sigma	Ref.: D9542
SmartBlockTM, 10mL		LOT:113E040r
Harris haematoxylin solution	Carl Roth	Ref.: X903.2
Vectashield Antifade Mounting Medium	Vectashield	Ref.: H1900

6.5. Antibodies

All antibodies used in this work are listed in Table 5 below.

Table 5: List of used antibodies, including manufacturer and reference- or LOT-number

Antibody	**Manufacturer**	**Reference- / LOT-number**
Ki-67 Recombinant Rabbit Monoclonal Antibody (0,031mg/mL)	Invitrogen	Ref.: MA-5-14520 LOT: ZG4390031
Rabbit IgG Isotype Ctrl (5mg/mL)	proteintech	LOT: XK366556
NanoSecAB anti-rabbit 647(0,5g/L)	Proteintech	Ref.: SrbAF647-01 LOT: 110082-01

6.6. Devices

All used devices are listed in Table 6 below.

Table 6: List of all used devices, including specification and manufacturer

Specification	**Manufacturer**	**Device**
WNB29	MEMMERT	Waterbath
IX73	Olympus	Microscope
HerasafeTM KS (NSF) Class II, Type A2 Biological Safety Cabinet	Thermo Scientific™	Sterile Hood
HeracellTM 150i CO2 Incubator	Thermo Scientific™	Incubator

Heraeus Megafuge 16R Centrifuge	Thermo Scientific™	Centrifuge
Serial number: VB201AL0000198	Starlab	Vortex
ABP 100-5DM	Kern	Scale
Mini fuge plus (Ref.: N2631-0017)	Starlab	Ep centrifuge
Infinite 200Pro	Tecan	Plate reader
0.0025mm2, 0.1mm depth	Marienfeld Brand GmbH	Counting chamber
BX53F	Olympus	Microscope
	Microtom	Cryostat

6.7. Software

All used software including the usage is shown in Table 7 below.

Table 7: List of used software, including their usage

Software	**Usage**
cellSens 2.2, Olympus	Phase contrast (PH) / Flurescence microscopy (FLM)
cellSens, Olympus	Haematoxylin/Eosin (H/E) imaging

7. METHODS

7.1. General Methods

7.1.1. Preparation of different solutions

7.1.1.1. Cell media

To prepare the medium for the cells, 50 mL of DMEM high glucose were first removed from the bottle. Then 50 mL of FCS and 5 mL each of penicillin-streptomycin and L-glutamine were added to the medium. Finally, the bottle was mixed well, and the prepared medium was aliquoted (CT-50 tubes). This medium was used for all cell lines.

7.1.1.2. Resazurin

The resazurin solution is required for the cell viability assay. As resazurin is overly sensitive to light, all work steps must be conducted with minimal exposure to light. All tubes and Eppendorf tubes (eppis) used were covered with aluminium foil or placed in the cabinet to protect them from light. Preparation began by weighing at least 5 mg of resazurin powder into an eppi (1.5 mL). The same amount of PBS in mL was prepared in a CT-15 for the dissolving step of the resazurin powder. A smaller amount of the prepared PBS was transferred to the eppi dissolving the resazurin powder and then transferred back to the CT-15. To ensure that the resazurin has completely dissolved, the tube must be vortexed for about ten seconds. Another CT15 tube containing 4500 µL PBS was prepared and 500 µL of the vortexed resazurin solution was added to gain a final concentration of 0.1 mg/mL. To ensure that the solution is homogeneously mixed, it must be vortexed again for a few seconds. A third CT15 tube, a sterile 10 mL syringe and a 0.2 µm PES sterile filter were then prepared for sterile filtration. The syringe was placed on the filter and held over the third CT15 tube while the freshly mixed resazurin solution was poured into the syringe and filtered. The concentration of the freshly prepared resazurin solution was 0.1 mg/mL. The tube must be protected from light until use.

7.1.1.3. Hoechst

This solution is required for live-dead staining and is very light-sensitive, which is why work must be done with minimal exposure to light.

The Hoechst stock solution (10 mg/mL) was taken from the -80°C freezer. For the Hoechst staining solution, a 160 µg/mL solution was prepared by transferring 300 µL of PBS to a 500 µL eppi and replacing 9.6 µL of the PBS by 9.6 µL of the stock solution. The solution was mixed before use and stored in the refrigerator when not in use.

7.1.1.4. Propidium iodide

This solution is also required for live-dead staining and is very light-sensitive, which is why work must be done with minimal exposure to light.

The propidium iodide (PI) stock solution (1 mg/mL) was taken from the refrigerator. A dilution of 1:2 is required for the PI staining solution. To prepare this solution, 150 µL of PBS was transferred to a 500 µL eppi and mixed with 150 µL of PI (in total 300 µL). This solution should also be stored in the refrigerator when not in use.

7.1.1.5. Antibodies

The antibodies were required for immunohistochemical (IHC) staining of spheroid sections.

Ki-67

Ki-67 was used as primary antibody and was prepared in two concentrations, 1:100 and 1:200. For this, 300 µL of blocking buffer were first added to a 500 µL eppi and 3 µL removed again. Subsequently, 3 µL of the Ki-67 stock solution (concentration 0.031 mg/mL) were added to achieve a concentration of 0.3 µg/mL (=1:100). For the 1:200 dilution, 100 µL of the 1:100 dilution were diluted further with 100 µL of blocking buffer.

Isotype-Control IgG

As a control for Ki-67, rat-IgG isotype control was used as a primary antibody and was required in a concentration of 1:10,000 to match the concentration of the Ki-67 antibody. The dilution was carried out in 2 steps. First, 500 µL of a 1:1000 dilution were prepared by adding 500 µL of blocking buffer and replacing 0.5 µL with the IgG stock solution (5 mg/ml) to obtain the 1:1000 dilution (5 µg/mL). To produce the required dilution, a 1:10 dilution of the previously prepared solution was made. For this, 20 µL of the 1:1000 dilution were diluted in 180 µL blocking buffer.

AlexaFluor 647 labelled secondary Antibody

NanoSecAB anti-rabbit AlexaFluor 647 was used as secondary antibody in a dilution of 1:1000. For this, 500 µL blocking buffer were added in a 500 µL eppi and 0.5 µL were replaced with 0.5µL of the secondary antibody AF 647.

Before the antibodies were used, they were first vortexed and then briefly spinned down to obtain a homogeneous solution.

7.1.2. Cell cultivation and seeding of Spheroids

7.1.2.1. Maintaining cells

The following steps were performed to maintain the cells in culture: Cells were cultured in a T75 cell culture flask and passaged twice a week (normally Mondays and Fridays). Under normal circumstances, the cells had a confluence of 80-95 % before passaging. For passaging, the old medium was first removed, and the cells were washed with PBS (5 mL). Tryp-LE (1.5 mL) was added to detach the cells, and the flask was incubated in the incubator (37°C) for 4 minutes. After incubation, the flask was washed a few times with fresh complete medium (7,5 mL in total). On the one hand, the medium is required to neutralise the Tryp-LE, and on the other hand, the cells are then brought into higher volume which can be further transferred. The cell suspension was transferred to a CT15 tube, which was then centrifuged for 5 minutes (200xg, RT). At the same time, a new T75 flask was labelled and filled with fresh, prewarmed-complete medium (12.5 mL). The supernatant was then discarded, and the cell pellet resuspended in 1 mL of fresh medium. Based on the cell line, a splitting ratio was estimated and according to this ratio a certain volume of the cell suspension was added to the new flask. A ∞-movement was performed to evenly distribute the cells in the new T75 flask, and the flask was placed back in the incubator until the next split.

7.1.2.2. Counting cells

For cell seeding, the same steps were carried out as described above. The resulting cell suspension was further diluted in fresh complete medium (1:20) for counting and two times 10 µL were then transferred to a Neubauer improved counting chamber. For accurate counting, it is important that each square contains at least 30 cells. The grid

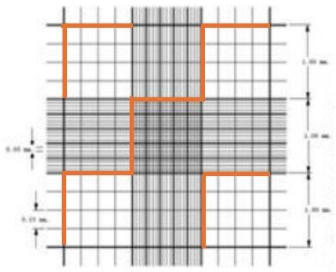

Figure 1: counting scheme

engraved in the counting chamber was used for orientation when counting. The counting was carried out as shown in Figure 1: Only the cells in the 4 corner chambers and the chamber in the middle were considered. Cells located on the orange lines were taken into consideration, while cells located on the other lines were excluded from the count.

The results of the individual chambers were then added together and multiplied by 20 (due to the 1:20 dilution). In this way, the cell concentration per mL is obtained. This allows to calculate the volume of the desired number of cells as indicated:

$$D / Z * C = N$$

D... desired cell counts per well

Z... calculated cells per mL in original dilution

C...Dilution needed to reach more than 20 µL

N... Volume needed per well

7.1.2.3. Seeding Spheroids

For seeding spheroids, 96-well round bottom ultra low attachment plates (BIOFLOAT Sarstedt) were used for each experiment. Before the cell suspension is added to the wells, the wells were filled with fresh prewarmed medium. The required volume is calculated as follows:

100µL – Volume cell suspension = needed Volume Medium

After the fresh medium was placed in the wells, the desired volume of cell suspension was added to the wells. Depending on what was planned for the experiment, either another 100 µL of medium or 100 µL of a collagen suspension were added (in total 200 µL). In the outer wells of the plate, 200 µL PBS were added to ensure the same conditions for each well.

The day on which the spheroids were seeded is called day 0 (D0).

7.1.3. Viability assay

The resazurin solution was prepared as described above in 7.1.1.2.

In the selected wells, all of the old medium was first removed and 108 µL of fresh medium were added. Subsequently, 12 µL of resazurin solution were added to each well (concentration of 0.01 mg/mL = 10 % resazurin/well) To distinguish the background signal from cell viability, the same was done in a control group of three wells containing

only media. Afterwards, the plate was placed back in the incubator for 4 h. After the incubation period, 100 µL of the supernatant were transferred to a clear 96 standard F-well plate, which was then covered with aluminium foil until readout. When the spheroids were reused, the resazurin supernatant remaining in the wells was removed and 200 µL of fresh medium were added.

A Tecan plate reader was used for the readout. The resazurin-based cell viability assay was generally performed every other day in the selected experiments.

7.1.4. Phase contrast microscopy

The spheroids in the wells were checked after seeding or at the latest on day 1 (D1). A 10x magnification and an exposure time of 15-20 ms were used on an epifluorescence microscope. Photos of the spheroids were taken and processed with the software cellSens 2.0.

Phase contrast photos were taken on the same days as resazurin assays were performed.

7.1.5. Live-dead staining and microscopy

7.1.5.1. Staining procedure

The required Hoechst and PI solutions were prepared according to 7.1.1.3. and **Error! Reference source not found.**..

Hoechst was used as it stains all cell nuclei and is visible in the FLM as a blue colour (emission wavelength = 461 nm) after excitation with fluorescent light.

The actual necrotic core of the spheroids was stained with PI, as it is not permeable to living cells and only affects the dead cells. In the FLM it appears as a yellow colour (emission wavelength = 617 nm) after stimulation.

The staining procedure was as follows: In the designated wells, 20 µL of the old medium were removed and discarded. Then 10 µL of the prepared Hoechst solution and 10 µL of the PI dilution were added to the wells, resulting in a total of 200 µL. The plate was then placed in the incubator for 2 h. After the incubation time, the stained spheroids were washed 3 times with PBS. To minimize the loss of spheroids, only 150 µL of the medium were discarded and 150 µL PBS were added for the washing steps. This must be done another 2 times to minimize a background signal when performing the readout.

7.1.5.2. Fluorescence microscopy

The readout was performed on a FLM. For Hoechst, the DAPI filter with an exposure time of 20 ms and a gain of 4.0 was used both for 2D images and for creating Z-stacks (images of the layers of the spheroids are taken at intervals of 5 µm). For PI, the Cy-3 filter with an exposure time of 10 ms and a gain of 4.0 was used for both. The captured images were also further processed with the cellSens 2.0 software. The necrotic core was stained and visualized on predetermined days.

7.1.6. Harvesting and embedding

To harvest spheroids, the medium was first removed from selected wells and spheroids were washed by adding approximately 200 µL of PBS. This process was repeated two more times, and the spheroids were then carefully transferred to prepared eppis using a 1 mL micropipette.

For embedding, the molds were first labelled and filled with a drop of tissue tek. The spheroids were then carefully removed from the eppi using a micropipette, placed in the tissue tek and excess PBS was carefully removed from the mold. The filled molds were then placed on dry ice until the tissue tek solidified. Once this was done, the molds were filled with tissue tek and allowed to harden again. Until the embedded spheroids were cut, they were stored in a -20°C freezer.

7.1.7. Sectioning of spheroids

When the embedded spheroids were to be cut, the desired spheroids were first removed from the freezer, the stamp was glued on to the samples with tissue tek and left to harden in the cryostat at -21°C. Once the tissue tek was solid, the spheroid was carefully removed from the mold and clamped in the cryostat. The settings for cutting were 6 µm cut and 20 µm for trim. Once everything was clamped and adjusted, the blade was carefully moved in the direction of the spheroid until an even piece of the surface was cut off. This may require further adjustment of the angle of the stamp.

The sections were carefully removed from the cut surface with a brush and picked up with a microscope slide. Up to 8 sections from one spheroid were placed on one microscope slide. Afterwards, the slides were labelled and stored in a -20°C freezer until needed for staining.

7.1.8. Haematoxylin and Eosin Staining

Haematoxylin/eosin staining should be performed to better visualize the cells and morphology of the spheroid sections on the slides.

For this purpose, the slides were first taken out of the freezer, placed on a piece of kitchen towel and the spheroids were circled with a histo-pen. Then the sections were covered with 4 % PFA for 7 minutes (not directly pipetted onto the spheroid) to fix the spheroids on the slides. The PFA was then removed without leaving any residue and the sections were washed twice with PBS for 3 minutes each to remove any remaining tissue embedding agent. For this purpose, the sections were placed in a small transparent container, which was carefully filled with PBS. After the 3 minutes, the PBS was poured away, the container was refilled with fresh PBS and left for another 3 minutes.

Before staining, the slides were placed in a slide holder and washed in a gentle stream of tap water for approximately one minute. Then the slides were stained with Mayer's haematoxylin for 30 seconds, followed by washing again with tap water for 20 seconds. In the next step, the slides were placed in NH_4OH for 20 seconds and then washed again with tap water for 1 minute. The resulting increase in pH causes the haematoxylin to turn blue. Furthermore, the sections were placed in eosin for about 30 seconds, which stains the acidophilic cell structures in different shades of red/pink. Finally, the excess eosin was washed off with tap water for about 10 seconds.

A series with ascending alcohol concentrations was used for dehydration. The slides were first immersed three times in 70 % ethanol, followed by three times in 96 % ethanol and finally three times in 100 % ethanol, each time for about one second. Afterwards, slides were immersed twice in xylene for one minute each time, then removed and allowed to dry. When the slides were completely dry, they were embedded with Entellan® to preserve the stained sections for light microscopy. Brightfield images of the stained spheroid sections were acquired using an Olympus microscope IX73 equipped with an Olympus DP-73 colour camera.

7.1.9. FL-labelled secondary Antibody Staining

Similar to the haematoxylin/eosin staining, the desired slides were first taken out of the freezer, placed on a paper towel and the spheroids circled with the histo pen (grease pencil). The sections were then covered with 4 % PFA for 7 minutes to fix them to the slides. The PFA was carefully pipetted into the circled areas. After the 7 minutes of incubation, PFA was carefully removed by pouring it into the waste CT-50 and tapping the edge on the paper towel to remove the remaining drops.

The slides were rinsed twice for 3 minutes by placing them in a container filled with PBS + 0.025 % Triton-x-100 to remove the tissue embedding medium and permeabilise the cell membranes. After the 3 minutes, the liquid was poured away, the container was

refilled slowly and left again for 3 minutes. After the second 3 minutes, the PBS was removed, and the slides were ready for staining.

For staining, the hydrophobic barriers were carefully dried with a Kimtech towel, and the slides were placed in a moist chamber lined with paper towels. Then 25 µl of blocking buffer was added to each spheroid and covered with an aluminium foil-wrapped lid for 60 minutes (to protect the sections from light). After the 60 minutes, the blocking buffer was tipped off and 25 µl of primary antibody dilutions were added on to the spheroid sections, which were prepared as described in chapter 7.1.1.5. The sections were then left for 120 minutes at room temperature or overnight at 4°C to allow the antibodies to bind.

After the incubation, the slides were washed twice for 3 minutes with PBS (without Triton) by pipetting the PBS onto the circled sections, tipping off after 3 minutes and repeating the procedure. Before adding the secondary antibody, the edges of the hydrophobic pencil were dried again if necessary. Afterwards, the secondary antibody was applied to each section and incubated again for 2 hours at room temperature. As the slides were stained with fluorescent dyes, work should be carried out as far as possible in the absence of light and the sections stored in the dark

After these 2 hours, the slides were washed again twice for 3 minutes, and the fat barriers were carefully dried again. Then 25 µL of 1:1000 DAPI dilution (stock conc. 1 mg/mL) were applied to each spheroid and left to incubate for 15-20 minutes at room temperature.

Finally, the sections were washed one last time with PBS twice for 3 minutes each and covered with Vectashield® mounting media and a coverslip. The edges were sealed with nail polish to avoid leakage of Vectashield®. The slides were stored in the dark at 4°C to prevent the fluorescent dye from burning out.

7.2. Optimization of monocellular breast cancer spheroids

7.2.1. MDA-MB-231-LM2-4 spheroid formation optimisation

7.2.1.1. Spheroid formation optimisation with collagen

First, MDA-MB-231 PGK eGFP luc cells were split and counted as described in chapter 7.1.2. The cells were then seeded as shown in Figure 2.

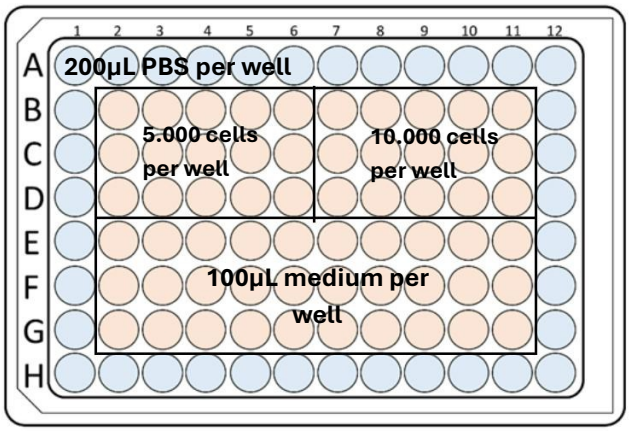

Figure 2: Seeding scheme of MDA-MB-231 PGK eGFP luc spheroids with collagen addition in different concentrations.

The cells were seeded in 100 µL medium and then incubated. On day 1, 100 µL of a 6 µg/mL collagen I solution was added to rows B and C. 100 µL medium was added to the remaining wells. From day 4 onwards, the medium was changed every 2nd day. 100 µL of medium were removed from all wells and replaced with new medium. Collagen was only added to rows B and C in the first week as shown below (Figure 3). In addition, viability assay was carried out on D4, D8, D11 and D15 as described in 7.1.3. 100 µL of transferred supernatant was then measured using the Tecan plate reader (Gain: 170). The empty wells containing spheroids were filled with fresh medium before the readout to protect them.

- Day 4:
  - Green:50µL 6µg/mL collagen
  - Violet: 100µL 6µg/mL collagen
  - Blue: just medium
  - Yellow: 50µL 6µg/mL collagen
- Day 6:
  - Green: 1:8 6µg/mL collagen
  - Violet: 100µL 6µg/mL collagen
  - Blue: just medium
  - Yellow: 50µL 6µg/mL collagen
- Day 8:
  - Green: just medium
  - Violet: 100µL 6µg/mL collagen
  - Blue: just medium
  - Yellow: 50µL 6µg/mL collagen

Figure 3: Different collagen additions each day for MDA-MB-231 PGK eGFP luc spheroids.

Daily phase-contrast images were taken with a light microscope as described in chapter 7.1.4. to record the growth.

Secondly, MDA-MB-231 LM2-4 eGFP luc cells were seeded the same way in the lower half of the plate as shown in Figure 4.

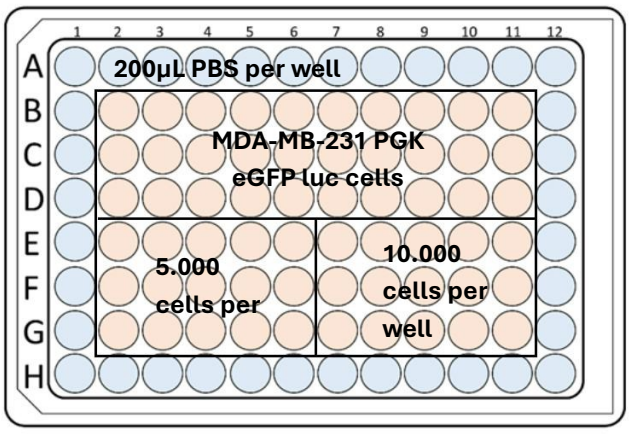

Figure 4: Seeding scheme of MDA-MB-231 LM2-4 eGFP luc spheroids with collagen addition in different concentrations.

The cells were also seeded in 100 µL medium and then incubated. On day 1, 100 µL of a 6 µg/mL collagen I solution was added to rows F and G. 100 µL medium was added to the remaining wells in row E. From day 4 onwards, the medium was changed every 2nd day. 100 µl of medium was removed from all wells and replaced with new medium. Collagen was only added to rows F and G in the first week as shown below (Figure 5). In addition, viability assay was carried out on D4, and D8, as described in 7.1.3. 100 µL of

transferred supernatant was then measured using the Tecan plate reader (Gain:170). The empty wells containing spheroids were filled again with fresh medium before the readout.

- Day 4:
  - Green:50µL 6µg/mL collagen
  - Violet: 100µL 6µg/mL collagen
  - Blue: just medium
  - Yellow: 50µL 6µg/mL collagen
- Day 6:
  - Green: 1:8 6µg/mL collagen
  - Violet: 100µL 6µg/mL collagen
  - Blue: just medium
  - Yellow: 50µL 6µg/mL collagen
- Day 8:
  - Green: just medium
  - Violet: 100µL 6µg/mL collagen
  - Blue: just medium
  - Yellow: 50µL 6µg/mL collagen

Figure 5: Different collagen addition each day for MDA-MB-231 LM2-4 eGFP luc spheroids

As described in Chapter 7.1.4, phase-contrast photos were taken daily with a light microscope to record the growth.

7.2.1.2. Comparison of LM2-4 eGFP luc spheroids with its wild-type cell line

In this experiment, the MDA-MB-231 LM2-4 eGFP luc was compared with its wildtype for which the cells were prepared for seeding as described in chapter 0. The two cell lines were seeded into a plate according to the scheme (Figure 6).

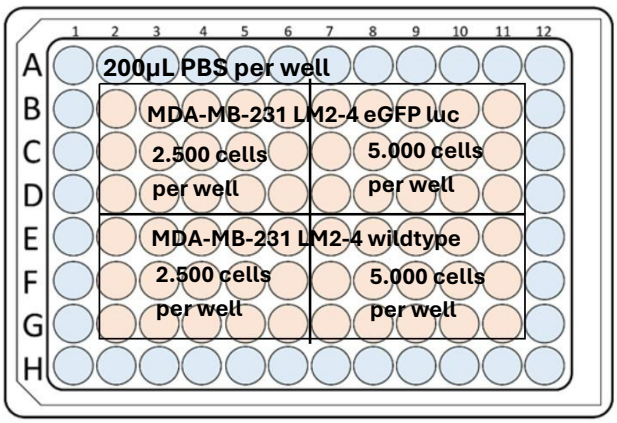

Figure 6: Seeding scheme der MDA-MB-231 LM2-4 eGFP luc and MDA-MB-231 LM2-4 wildtype spheroids with collagen addition in different concentrations.

From day 4 onwards, the viability assay was performed every second day as described in chapter 7.1.3. For this purpose, the resazurin solution was prepared as described in chapter 7.1.1.2. The entire rows B and E were used for the assay. Tecan read out was performed with optimal gain, gain 170 and 150. The later two were used to analyse the results of the assay. Medium was changed each time after the resazurin assay. In doing so, 100 µL medium was removed from the wells and replaced with 100 µL fresh medium.

In addition, before each resazurin assay, phase contrast images were taken as described in chapter 7.1.4 to record the growth.

7.2.2. Optimisations of MDA-MB-231 spheroids

7.2.2.1. MDA-MB-231 PGK eGFP luc spheroids with different collagen concentrations and centrifugation

MDA-MB-231 PGK eGFP luc cells were prepared for seeding as described in chapter 0. and then 5,000 cells per well were seeded in 100 µL medium into the entire plate,

excluding the outer wells. The wells at the very edges were filled with 200 µL PBS to give all spheroids the same conditions.

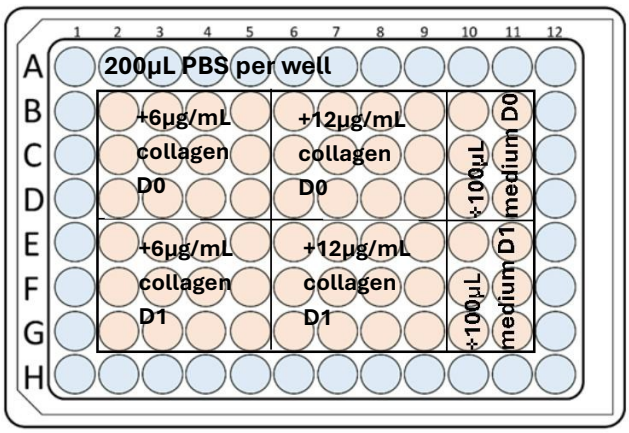

Figure 7: Scheme of collagen addition in different concentrations and on different days.

Afterwards, on the day of seeding (D0), 100 µL of 6 µg/mL, 12 µg/mL or only medium were added to rows B, C and D, as shown in Figure 7. 2.5 hours after the addition, the plate was centrifuged for 3 minutes at 300g. On day 1, the different collagen concentrations were added to the remaining lower 3 rows (E, F and G) and the plate was again centrifuged for 3 minutes at 300g.

From day 4 onwards, a resazurin assay was performed every other day, as described in section 7.1.3. The resazurin solution was prepared as described in section 7.1.1.2. The wells of the complete rows B and E were used for the assay. For the read-out with the plate reader, optimal gain was used first, followed by gain 170. The medium was changed every other day after the resazurin assay by removing 100 µL of the old medium and replacing it with fresh medium. After each medium change, the plate was centrifuged at 300 g for 3 minutes.

On days 0 and 1, as well as before each resazurin assay, phase contrast photos were taken as described in section 7.1.4..

To see whether the results of this experiment in Chapter 7.1.5 are reliable, this experiment was repeated a second time exactly as described above.

7.2.2.2. Visualisation of living and dead cells in MDA-MB-231 PGK eGFP luc spheroids with different collagen concentrations

MDA-MB-231 PGK eGFP luc cells were prepared for seeding as described in chapter 0. and 5000 cells per well seeded in the entire plate, excluding only the outer wells. The wells at the very edge of the plate were filled with 200 µL PBS to ensure uniform conditions.

The different collagen concentrations were then added to the wells similarly as described previously (Figure 8). The plate was then centrifuged at 300g for 3 minutes and incubated afterwards.

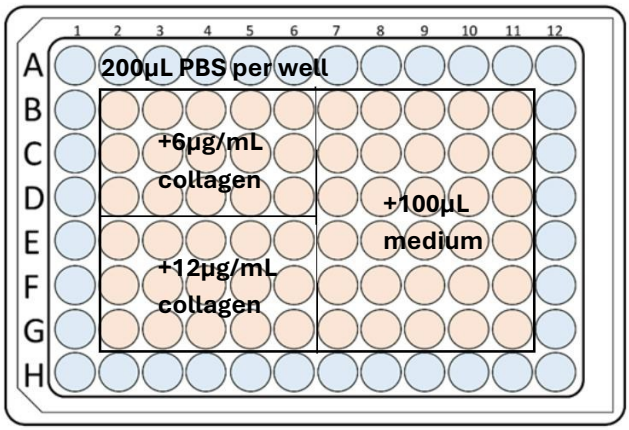

Figure 8: Schematic representation of the addition of different collagen concentrations.

On day 1, the staining solutions were prepared as described in sections 7.1.1.3 and **Error! Reference source not found.**. and the selected wells, as illustrated in Figure 9, were stained as described in chapter 7.1.1.5.

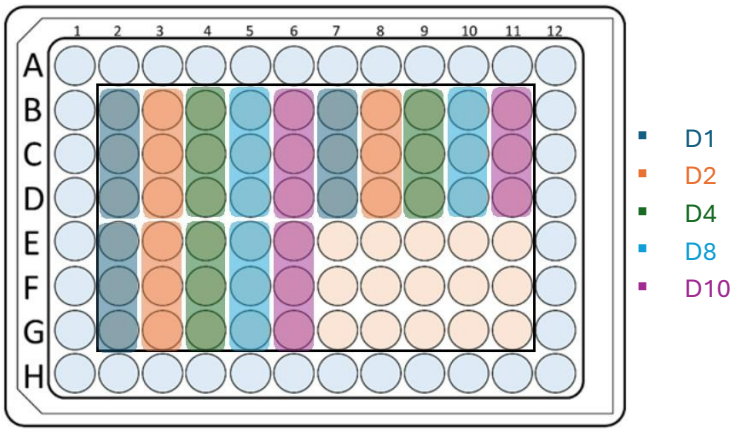

Figure 9: Schematic representation of the wells used for live/dead staining on different days.

After the 2 hour incubation period, the stained spheroids/cell aggregates were washed with PBS as described in chapter 7.1.5.1. The wells were then analysed and photographed using a fluorescence microscope as described in section 7.1.5.2.

The live-dead assay was repeated on days 2, 4, 8, and 10.

7.2.2.3. MDA-MB-231 PGK eGFP luc spheroids with basement membrane matrix

MDA-MB-231 PGK eGFP luc cells were seeded in a count of 5000 cells per well in 100 µL as described in chapter 0. The wells at the very edge were again filled with 200 mL PBS. Different Geltrex® concentrations were then added to the wells, as shown in the diagram below (Figure 10). The Geltrex® was compared with 6 µg/mL collagen to determine direct differences. Afterwards, the plate was centrifuged for 3 minutes at 300 g. The next day, Geltrex® was again added to the lower left area and the plate was gently shaken for 15 minutes (at around 100 rpm).

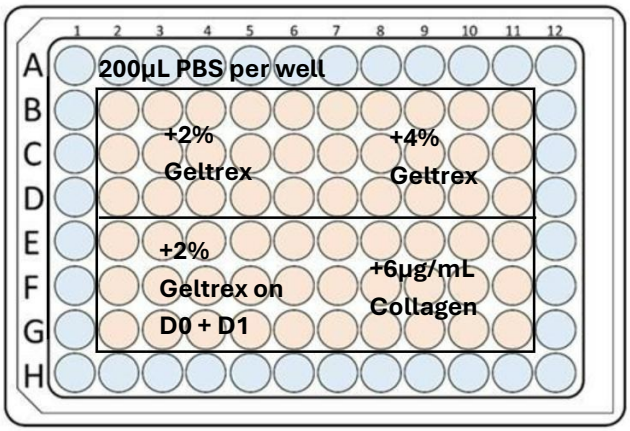

Figure 10: Schematic of the different Geltrex concentrations.

After a short waiting period, the live-dead staining was started immediately as described in chapter 7.1.5. For this, two spheroids per concentration were always used as shown in Figure 11. Life dead staining was repeated on days 4, 8 and 11.

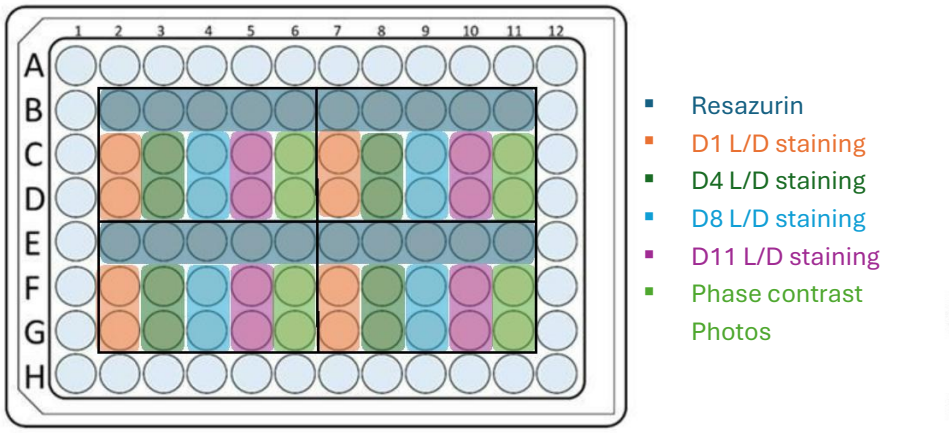

Figure 11: Graphic illustration of the use of wells.

From day 4 onwards, a resazurin assay was also performed every 2nd day as described in chapter 7.1.3. and phase contrast photos were taken as described in chapter 7.1.4.

After analysing the life dead staining, the spheroids used were harvested and embedded in tissue tek as described in chapter 7.1.6. The embedded spheroids were later cut as described in chapter 7.1.7. and placed on slides for subsequent H/E staining (chapter 0.).

In a second experiment, cell lines MDA-MB-231 PGK eGFP luc and additionally MDA-MB-231 LM2-4 eGFP luc were prepared for seeding as described in section 0. Half of the plate was seeded with 5000 cells per well in 100 µL of the first cell line and the other half with 5,000 cells per well in 100 µL of the second cell line. This time, lower concentrations of Geltrex® were added to the plate (Figure 12). The plate was then centrifuged for 3 minutes at 300g. The next day, Geltrex® was added again, and the plate was shaken gently for 15 minutes (around 100 rpm). All following steps including viability assay, live-dead staining, cryo-sectioning and H/E staining were carried out the same way as described above.

Additional sections were also stained with fluorescent secondary antibodies as described in section 7.1.9 and then analysed using FLM. Cy5 (50 ms), Cy3 (200 ms), DAPI (200 ms), and PH (20 ms) filters were used, and the images of the channels were then overlaid.

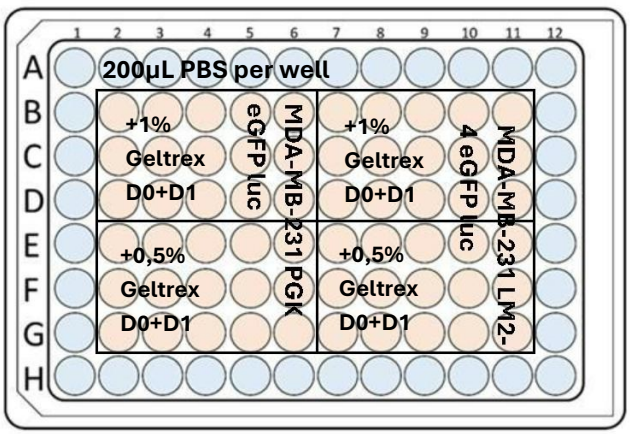

Figure 12: Scheme of the Geltrex addition.

7.3. Multicellular breast cancer spheroids

Another way to optimize the spheroid formation of the cell lines MDA-MB-231 PGK eGFP luc and MDA-MB-231 LM2-4 eGFP luc is to co-culture them with fibroblasts. The fibroblast cell line HMF3S was used for this purpose. For multicellular breast cancer

spheroid model, MDA-MB-231 PGK eGFP luc or MDA-MB-231 LM2-4 eGFP luc were seeded with human mammary fibroblast cell line HMF3S. All three cell lines were

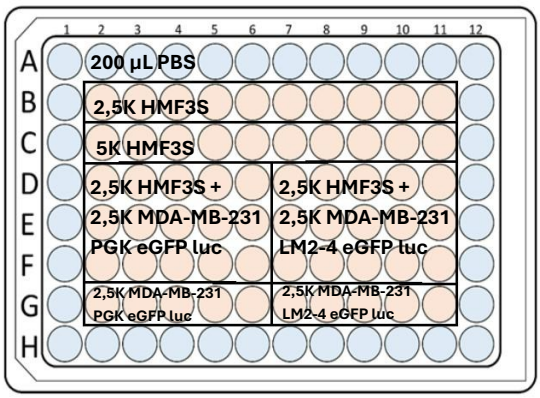

Figure 13: Schematic representation of the distribution of different cell lines in the plate.

prepared for seeding as described in section 0. They were then added into the wells of the plate consecutively (one cell line at the time) as shown in Figure 13. From day 4 onwards, a viability assay was performed every other day (chapter 7.1.3). On days 4, 7, 10, 12, and 14, live-dead staining was also performed (see chapter 7.1.5) (Figure 14).

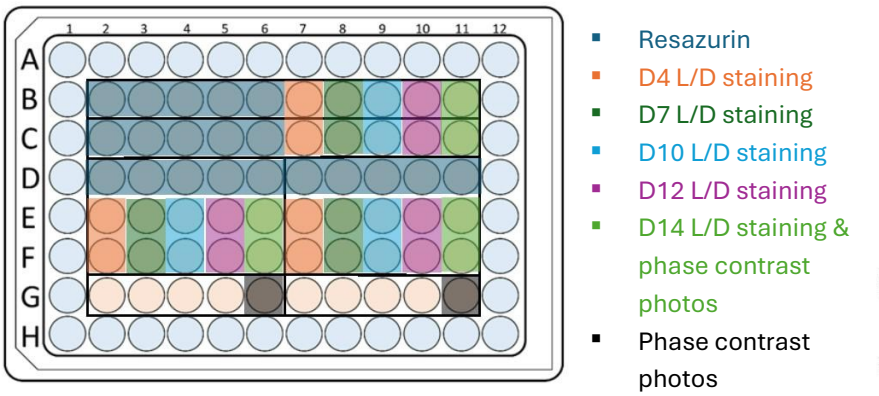

Figure 14: Scheme of the use of wells for live-dead staining, resazurin assay, and phase contrast photos.

After evaluating the live-dead staining, the spheroids used were harvested and embedded as described in chapter 7.1.6. Since the spheroids had already been washed with PBS before the L/D staining was evaluated, this step could be skipped during harvesting. After embedding, the spheroids were cut as described in chapter 7.1.7 and selected sections of each cell combination were stained with haematoxylin/eosin (chapter 0). These H/E-stained sections were then photographed with a light microscope.

Further cuts were stained immunohistochemically for Ki-67 with a fluorescence-labelled secondary antibody as described in chapter 7.1.9. The stained sections were

then analysed and imaged using a FLM. For this purpose, the filters Cy5 (50 ms; range 0-7,000), Cy3 (200 ms; range 0-10,000), DAPI (200 ms; range 0-7,000), and PH (20 ms; range 0-7,000) were used, and the respective photos were overlaid.

8. RESULTS AND DISCUSSION

The results of the experiments in this master's thesis were structured according to the experimental setup.

8.1. Optimization of monocellular breast cancer spheroids

8.1.1. MDA-MB-231-LM2-4 spheroid formation optimisation

8.1.1.1. Spheroid formation optimisation with collagen

The aim of this experiment was to optimize spheroid formation of the cell line MDA-MB-231 LM2-4 by adding collagen. For this purpose, MDA-MB-231 PGK eGFP luc cells (as a "positive" control") and MDA-MB-231 LM2-4 eGFP luc cells were seeded into a plate in densities of 5,000 and 10,000 cells per well. Collagen at a concentration of 6 µg/mL was then added to half of the wells per cell population (final concentration of 3 µg/mL). Phase contrast photos were taken every day to document cell growth.

As it can be seen in Figure 15, collagen has no effect on the compactness of cell aggregation in MDA-MB-231 LM2-4 eGFP luc cells. Both the cell clusters with 5,000 and 10,000 cells are too large to be completely captured in the phase contrast photo within a very short time. It also appears that these cell clusters form a blanket at the bottom of the well rather than a spheroid or cell aggregate.

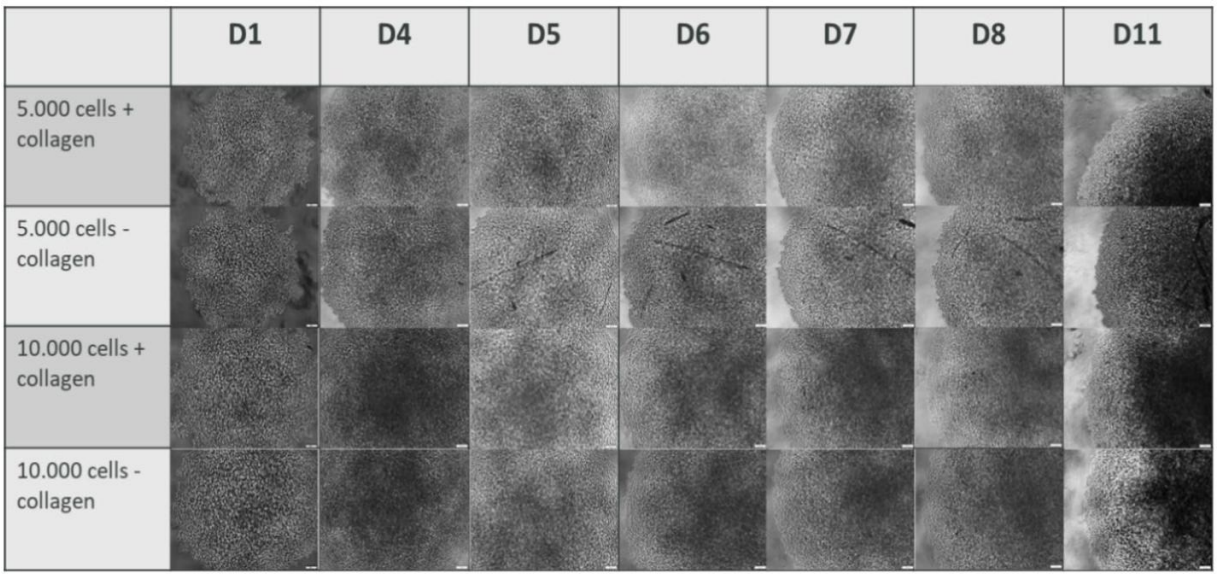

Figure 15: Phase contrast microscope images of MDA-MB-231 LM2-4 eGFP luc spheroids from two cell counts (5,000 and 10,000) at different growth times, according to the specified time points. One spheroid per cell concentration +/- collagen is shown as an example of n=5 spheroids. D=day; images were taken with exposure of 15 ms, 10x magnification, scale bar: 100 µm

Figure16 shows that the MDA-MB-231 PGK eGFP luc cells to which collagen was added form a slightly more compact cell cluster in the first week than the cells without collagen. After this week, the collagen probably has been diluted to such an extent that it has lost its effect on the cells. However, true spheroids are not formed for neither of

the cell lines because the cells are too loosely connected to each other, both with and without collagen.

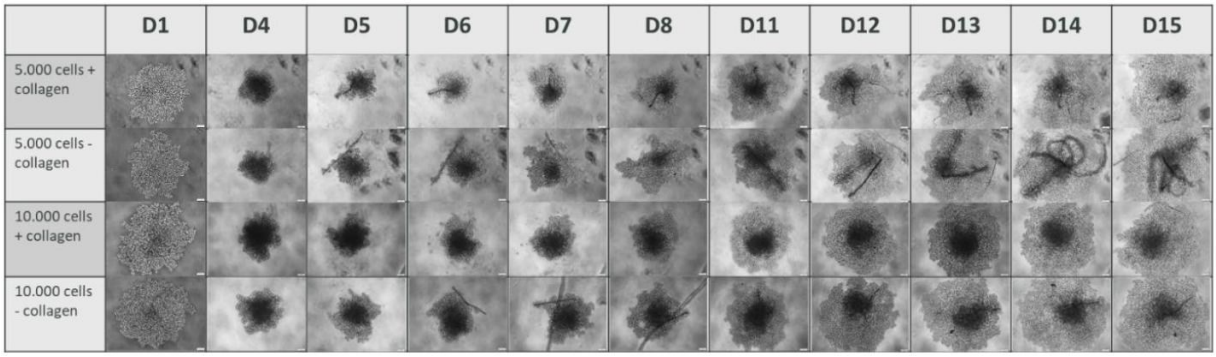

Figure 16: Phase contrast microscope images of MDA-MB-231 PGK eGFP luc spheroids from two cell counts (5,000 and 10,000) at different growth times, according to the specified time points. One spheroid per cell concentration +/- collagen is shown as an example of n=5 spheroids; D=day; images were taken with exposure of 15 ms, 10x magnification, scale bar: 100 µm.

In addition to the photo documentation, a viability assay was planned to be performed every other day starting on day 4. Due to problems with resazurin production, the data from day 6 could not be included.

Figure 17 shows that the cell aggregates from the cell line MDA-MB-231 PGK eGFP luc without collagen seem to have a slightly higher growth rate than the cells with collagen from the outset. As already seen in Figure 16, the resazurin assay also shows that the cells grow more strongly from day 11 onwards. This applies to both seeding concentrations and to cells with and without collagen addition. The fact that the collagen group showed slightly less viability signal than those without collagen could be due to the collagen addition.

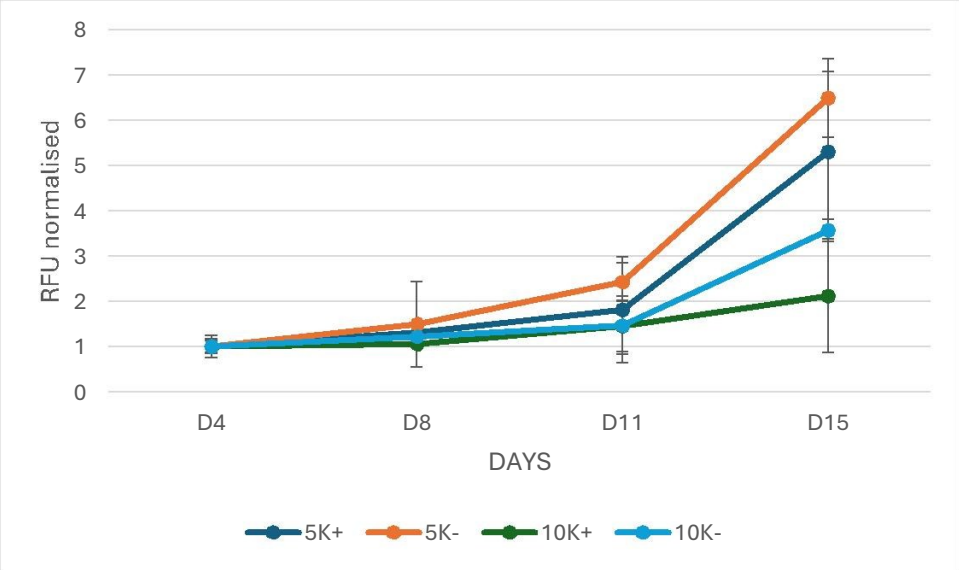

Figure 17: Average fluorescence signal (RFU) by resazurin cell viability assay of MDA-MB-231 PGK eGFP luc spheroids with an initial seed count of 5K (= 5,000) and 10K (= 10,000) cells. The RFU shown is the average of N=5 spheroids (one measurement per spheroid) and normalised to the first measurement (=D4). D=day.

Furthermore, the viability assay was discontinued after day 8 at the cell line MDA-MB-231 LM2-4 eGFP luc because the cell clusters became too large and exceeded the upper measurement limit of the evaluation at gain 170. The gain refers to the signal amplification factor in the used Tecan reader's detector and determines the sensitivity and dynamic measurement range.

Figure 18 shows, just like the phase contrast photos before, the huge growth of the cells (normalised to the first measurement). The cell clusters with 5,000 cells per well grow a more than the cell aggregates with 10,000 cells per well within four days, which is

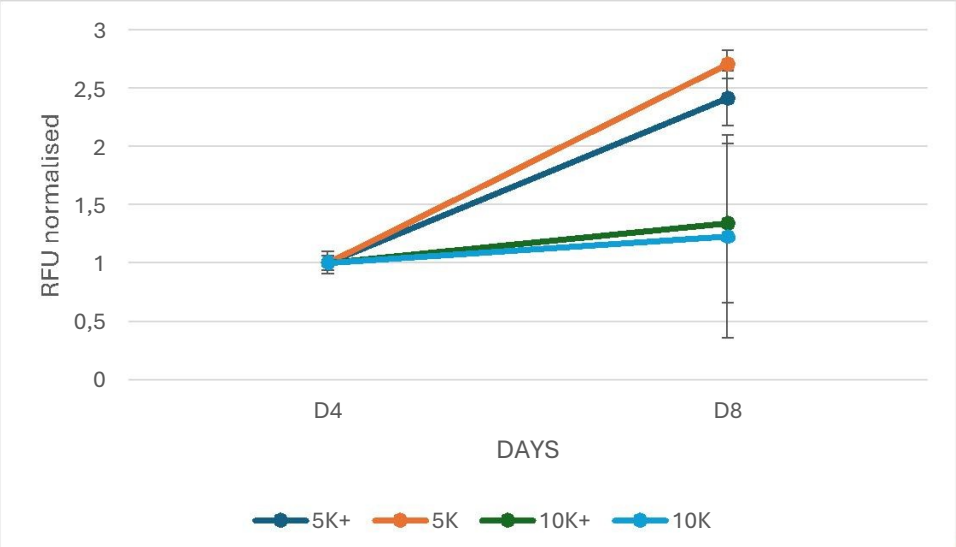

Figure 18: Average fluorescence signal (RFU) by resazurin cell viability assay of MDA-MB-231 PGK eGFP luc spheroids with an initial seed count of 5K (=5,000) and 10K (=10,000) cells. The RFU shown is the average of N=5 spheroids (one measurement per spheroid) and normalised to the first measurement (=D4). D=day.

illustrated in the graph. The MDA-MB-231 LM2-4 eGFP luc cell aggregates with collagen show no difference in growth or compactness compared to the ones without addition of collagen.

8.1.1.2. Comparison of LM2-4 eGFP luc spheroids with its wild-type cell line

In this experiment, the aim was to compare the MDA-MB-231-LM2-4 eGFP luc cell line with its wildtype to exclude any malfunction in spheroid formation due to the genetic modification. The MDA-MB-231 LM2-4 eGFP luc cells were transduced with lentiviruses encoding eGFP luc (48). However, not all cells in this culture are transfected with eGFP luc. Both cell lines were seeded in the same way simultaneously, and the resazurin assay and phase contrast imaging were performed.

The phase contrast photos (Figure19) show that the cell aggregates grew rapidly in a very short time. However, both cell lines show a similar density of cell clusters, suggesting that this species does not voluntarily form spheroids and the insertion of eGFP luc has no effect on that. The only difference that can be seen is that the cell clusters seeded with 5,000 cells are more densely packed than those with 2,500 cells.

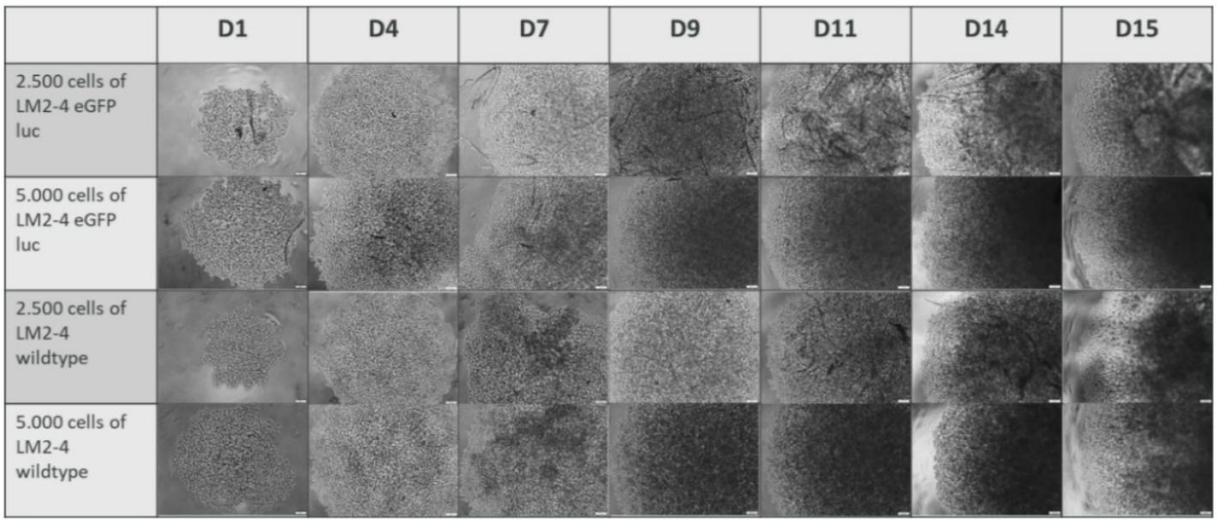

Figure 19: Phase contrast microscope images of MDA-MB-231 LM2-4 eGFP luc spheroids and MDA-MB-231 LM2-4 wildtype from two cell counts (2,500 + 5,000) at different growth times, according to the specified time points. One spheroid per cell concentration +/- collagen is shown as an example of n=5 spheroids. D=day; images were taken with exposure of 15 ms, 10x magnification, scale bar: 100 µm.

The evaluation of the viability assay (Figure 20) also clearly shows the rapid growth of these cell lines. However, the growth of the groups seeded with 5,000 cells is both slower and, in the case of the MDA-MB-231 LM2-4 eGFP luc spheroids, also slightly decreases towards the end, suggesting a plateau in growth.

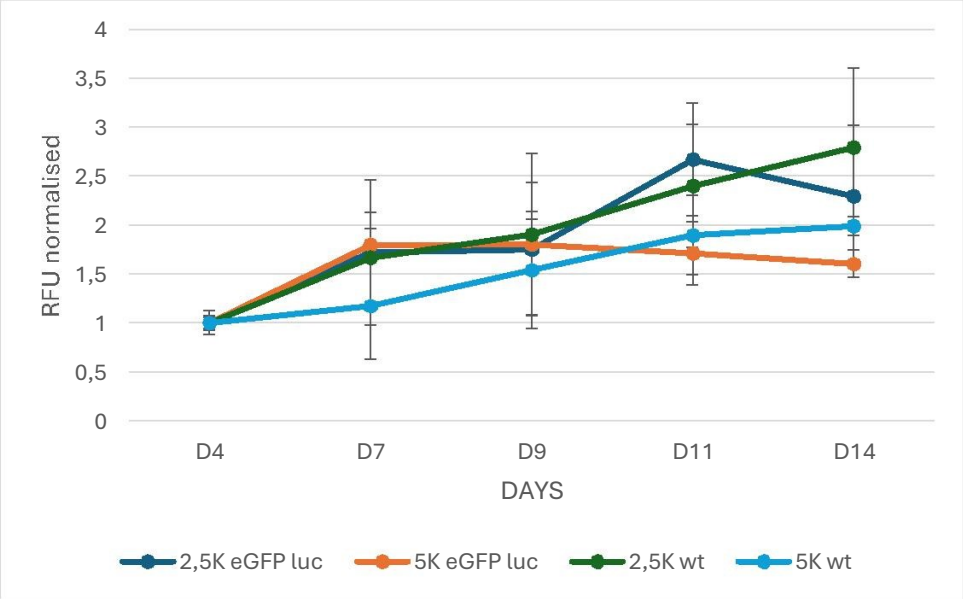

Figure 20: Average fluorescence signal (RFU) by resazurin cell viability assay of MDA-MB-231 LM2-4 eGFP luc (=eGFP luc) and MDA-MB-231 LM2-4 wildtype (=wt) spheroids with an initial seed count of 2,500 (=2.5K) and 5,000 (=5K) cells. The RFU shown is the average of N=5 spheroids (one measurement per spheroid) and normalised to the first measurement (=D4). D=days.

8.1.2. Optimisations of MDA-MB-231 spheroids

As the MDA-MB-231 cell line and their derivates did not form proper spheroids even though the used protocols suggested otherwise (67,68), the following experiments were focused on the establishment of proper spheroids from this cell line.

8.1.2.1. MDA-MB-231 PGK eGFP luc spheroids with different collagen concentrations and centrifugation

The aim of these experiments was to determine whether different concentrations of collagen and the timing of its addition have an influence on spheroid formation of MDA-MB-231 PGK eGFP luc. Additionally, centrifugation of the plate was introduced, as it was found in a protocol (69). For this purpose, 6 µg/mL or 12 µg/mL collagen were added to the cells either on day 0 or day 1 and then centrifuged. Phase contrast photos were taken on days 0, 1, 2, 4, 7, 9, 12, 14, and 16 to document spheroid formation and growth (Figure 21).

Figure 21 shows that the cell aggregates remain relatively compact until around day 9, afterwards the compact cell clusters begin to loosen up again. The addition of collagen directly on day 0 results in longer-lasting compactness of the cells than the addition on day 1. The spheroids that received only medium were also more compact on day 0 than those receiving the second half of media on day 1.

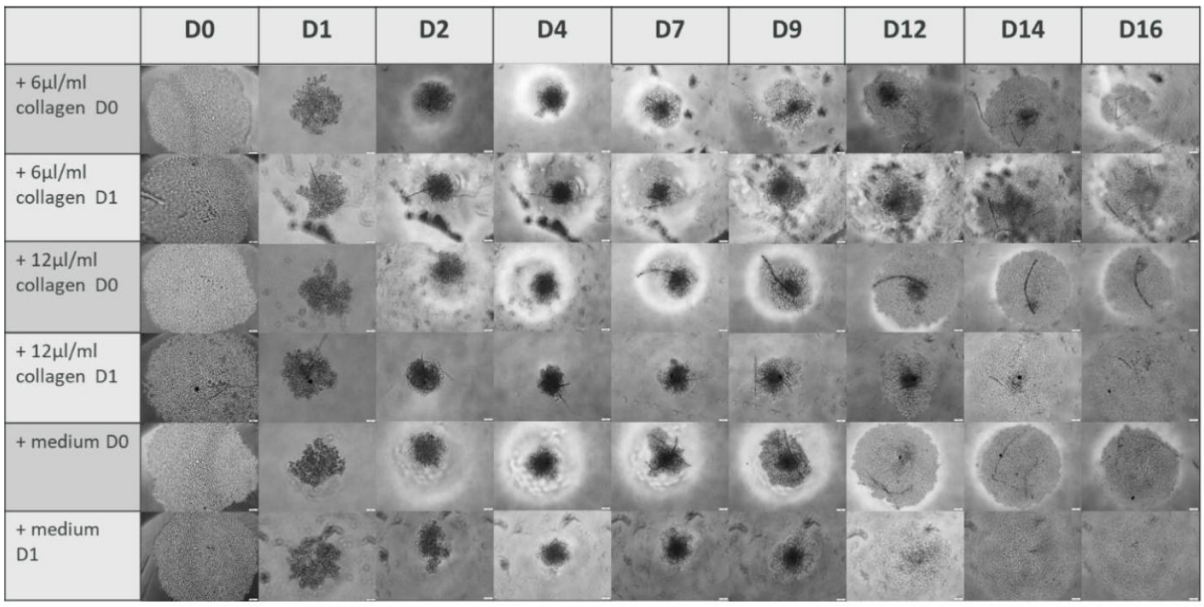

Figure 21: Phase contrast microscope images of MDA-MB-231 PGK eGFP luc spheroids from one cell count (5,000) at different growth times, according to the specified time points. One spheroid per collagen concentration (+ 6 µg/mL or 12 µg/mL collagen) or only medium (D0 and D1) is shown as an example n=5 spheroids. D=day; images are taken with exposure of 15 ms, 10x magnification, scale bar: 100 µm.

The evaluated resazurin assays also show linear cell growth until day 9, after which the signal begins to decline in all cases (Figure 22). The loosening of the spheroids may therefore be due to the cells slowly beginning to die off, forming a corona of dead cells.

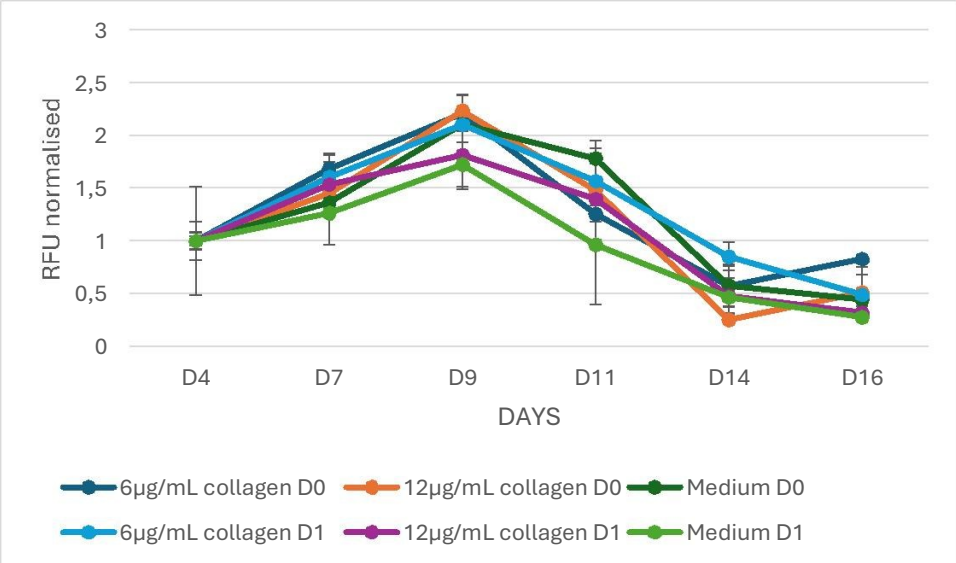

Figure 22: Average fluorescence signal (RFU) by resazurin cell viability assay of MDA-MB-231 PGK eGFP luc spheroids with an initial seed count of 5,000 cells and different collagen concentration at different addition times. The RFU shown is the average of N=4 (only medium n=2) spheroids (one measurement per spheroid) and normalised to the first measurement (=D4). D=day.

Both Figure 21 and Figure 22 show images from the first attempt of the experiment, as the days of the second experiment do not correspond exactly to the days of the first experiment. The images from the second experiment can be found in the appendix.

8.1.2.2. Visualisation of living and dead cells in MDA-MB-231 PGK eGFP luc Spheroids with different collagen concentrations

The aim of this experiment was to document the progression of cell death over the time using live-dead staining. For this purpose, two different concentrations (6 µg/mL or 12 µg/mL) of collagen were used again and compared with cells treated with medium only. Figure 23 shows that all cell nuclei were stained blue using Hoechst. The propidium iodide only stained the dead cells orange-red viusalised in yellow, as their cell membranes are permeable for PI compared to those of living cells. The cells can be visualised with FLM (shown in green) as they have been previously stably transduced with eGFP luc as described in Billerhart et. al and Wang et. al (48,66) . Until about day 8, only a few dead cells can be found. On day 11, there are already quite a few more. It is interesting to note that the dead cells are more prevalent among the eGFP-labelled cells. This may indicate that these modified cells have a shorter lifespan than the unlabelled ones. Furthermore, these images also suggest that the cells grow rather in a 2D sheet than a spheroid, as the typical necrotic core cannot be observed.

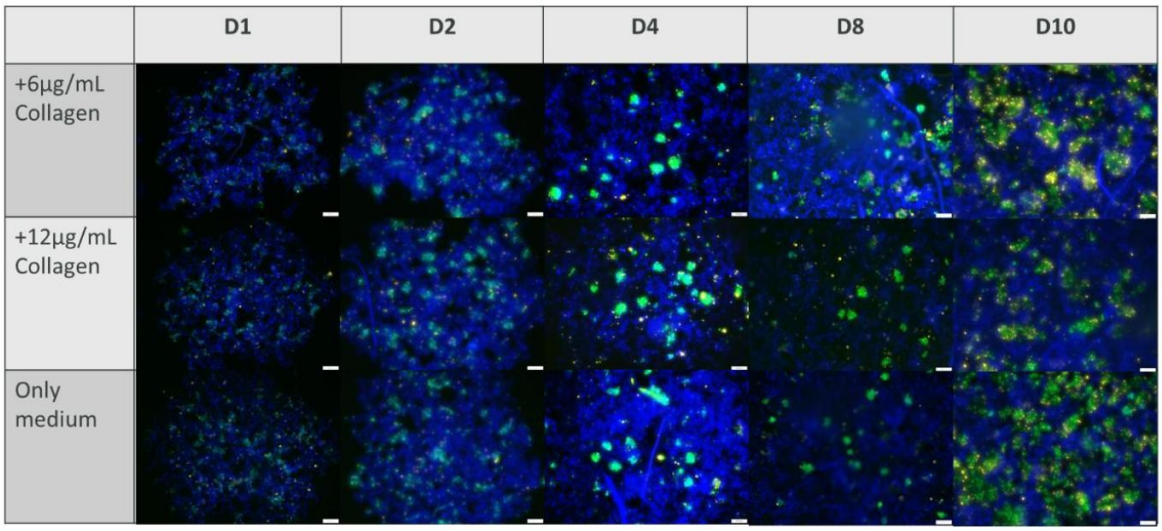

Figure 23: Necrotic core staining of 5K (=5,000) MDA-MB-231 PGK eGFP luc spheroids via fluorescence microscopy (FLM). Spheroids were stained with Hoechst and PI (2 hour incubation time). Images were captured as Z-stacks (exposure time for Hoechst=20 ms with DAPI filter, conc. 16 µg/mL; exposure time for PI=10 ms with Cy3 filter, conc. 0.5 mg/mL; exposure time for the FITC filter =20 ms to visualise the eGFP labelled cells) and the maximum projection was extracted. The shown images show one out of n=3 spheroids. D=day. Scale bar: 100 µm.

8.1.2.3. MDA-MB-231 PGK eGFP luc spheroids with basement membrane matrix

As the addition of collagen I did not lead to sufficient spheroid formation, Geltrex® was used as a basement membrane matrix in the next approach (70). Unlike collagen I, Geltrex® consists of a complex, gel-like mixture of various extracellular matrix proteins (e.g. laminin, collagen IV, enactin/nidogen and heparan sulphate proteoglycans). This

allows it to simulate a natural basal lamina matrix and support cell adhesion in 3D cultures (71). For this, the entire plate was seeded and then mixed with a specific concentration of Geltrex® or Collagen I (as a control). The plate was then centrifuged and incubated. The next day, Geltrex® was added to some of the wells again and the plate was gently shaken shortly.

Phase contrast photos were taken on days 1, 4, 6, 8, 11, 13, 15 and 18 to document spheroid formation and cell growth (Figure 24). The addition of Geltrex® in all concentrations leads to compact spheroids with a clear border up to day 11. After that, a corona of not very compact cell aggregates forms around the spheroids. In comparison, collagen I only leads to a loose cell aggregate with a slightly more compact core, which lasts until day 8.

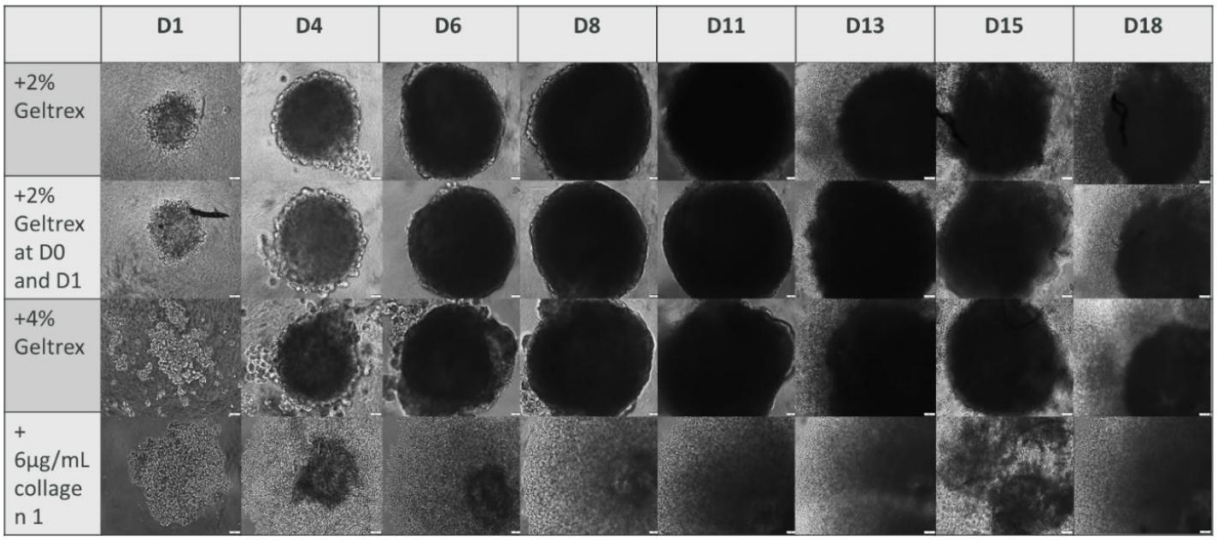

Figure 24: Phase contrast microscope images of MDA-MB-231 PGK eGFP luc spheroids from one cell count (5,000) at different growth times, according to the specified time points. One spheroid of each Geltrex® concentration (2 %, 2x2 %, 4 %) and +6 µg/mL collagen I is shown as an example n=5 spheroids. D=day; images with exposure of 15 ms, 10x magnification, scale bar: 100 µm.

The experiment was repeated with lower Geltrex concentrations and additionally with the cell line MDA-MB-231 LM2-4 eGFP luc. Phase contrast photos were also taken here (Figure 25) show that adding 1 % Geltrex twice to both cell lines results in compact spheroids with a clear border that persist until day 6. From day 8 onwards, as explained above, a corona of cells forms and the spheroid loosens its shape. In wells to which only 0.5 % Geltrex was added twice, a slightly denser core forms in the cell aggregate from day 6 onwards, which dissolves again from day 11 onwards. However, no proper spheroid are formed with this lower concentration.

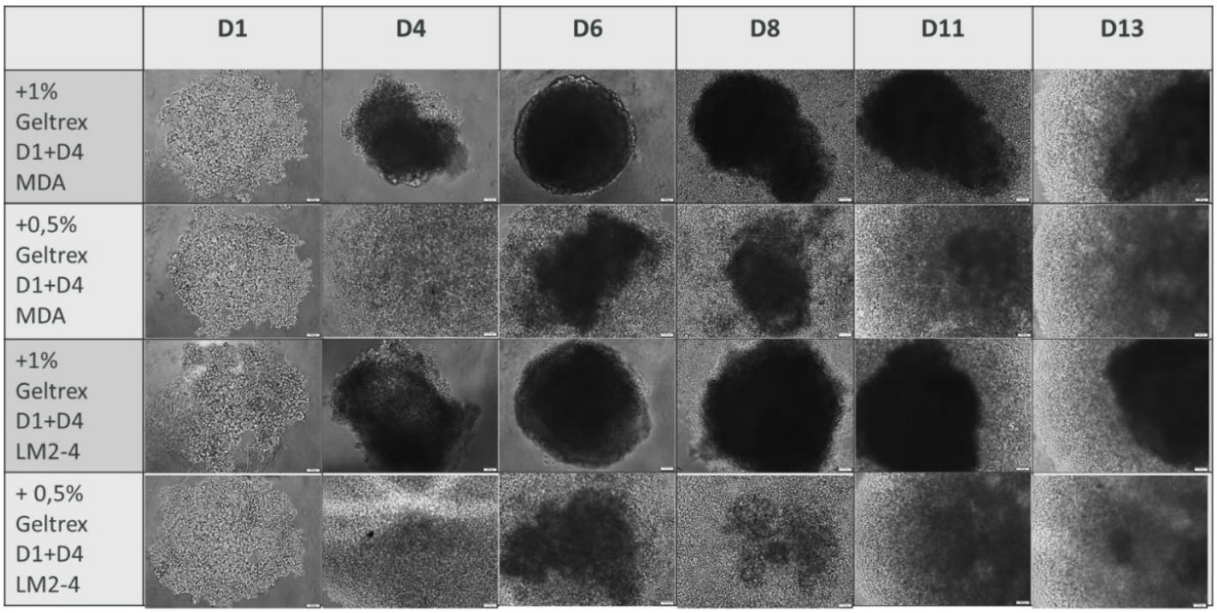

Figure 25: Phase contrast microscope images of MDA-MB-231 PGK eGFP luc and MDA-MB-231 LM2-4 eGFP luc spheroids from one cell count (5,000) at different growth times, according to the specified time points. One spheroid of each Geltrex® concentration (2x1 % and 2x0,5 %) is shown as an example n=5 spheroids. D=day; images with exposure of 15 ms, 10x magnification, scale bar: 100 µm.

In addition, a viability assay was performed every other day starting on day 4 to document cell growth for both experiments (Figure 26 and Figure 27).

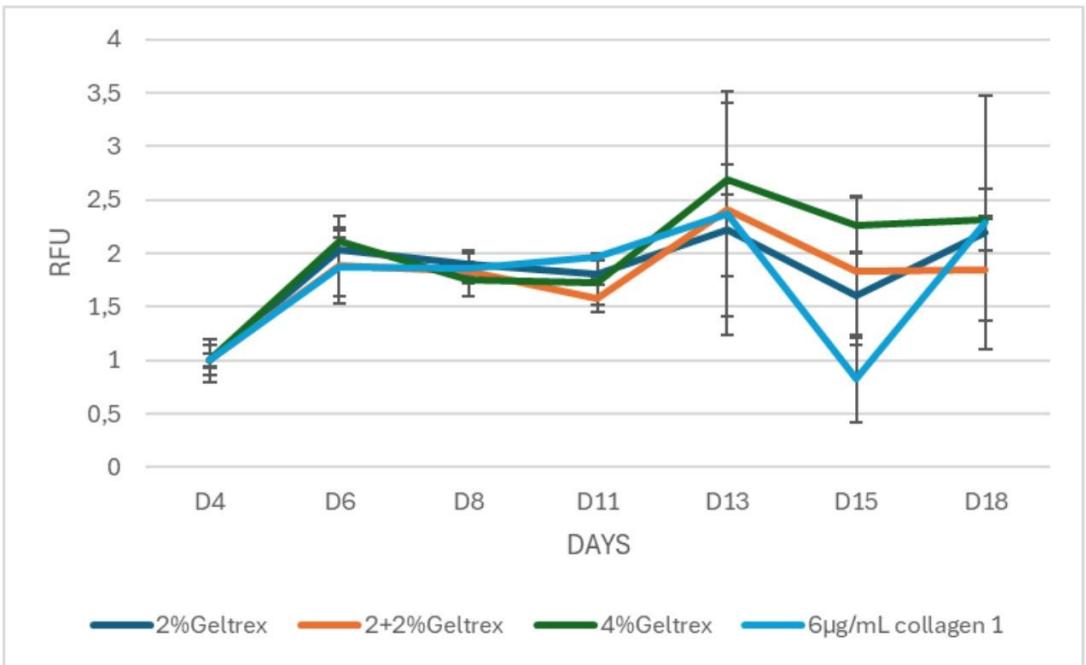

Figure 26: Average fluorescence signal (RFU) by resazurin cell viability assay of MDA-MB-231 PGK eGFP luc spheroids with an initial seed count of 5,000 cells and addition of different Geltrex concentrations or Collagen I. Read out was performed at different time points. The RFU shown is the average of N=5 spheroids (one measurement per spheroid) and normalised to the first measurement (=D4). D=day.

The spheroids initially grow quite rapidly and then remain virtually unchanged. Only when the corona forms to increase cell growth become apparent again. This could be attributed to the fact that, from this day onwards, the Geltrex® concentration is too low to keep the cells in their dense spheroid form. After day 13, cell growth largely stagnates.

The evaluation of the resazurin assays from the second experiment also shows similar behaviour, strong initial growth from day4 to day 6, which then remains constant. Only when the corona forms the cell growth increases again. Additionally, similar behaviour can be observed between the different concentrations and cell lines. (Figure 27)

Aside from the viability assay, a necrotic core assay was also conducted on days 1, 4, 8, and 11. Figure 28 shows the results of the necrotic core staining. Unfortunately, the spheroids were lost during the washing process on day 1. On day 4, very few dead cells (illustrated in yellow) can still be seen, mainly located inside the spheroids. From day 8 onwards, the proportion of dead cells increased significantly. Spheroids receiving collagen I also showed a sharp increase in dead cells from day 8 onwards, which were increasingly found in the eGFP-labelled cells. This could be because the labelled cells may have a slightly shorter lifespan than the unlabelled cells.

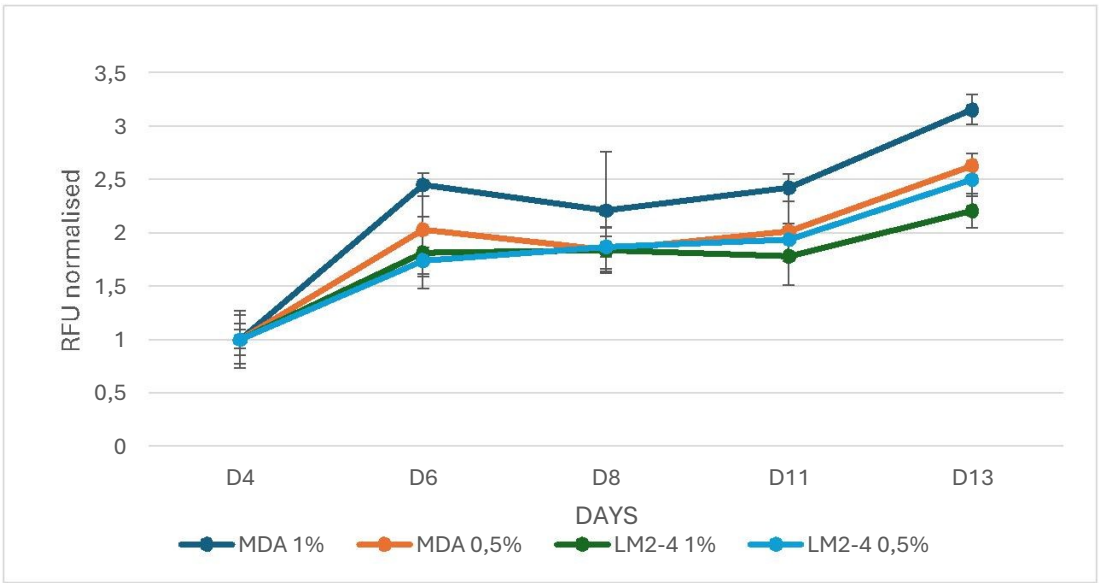

Figure 27: Average fluorescence signal (RFU) by resazurin cell viability assay of MDA-MB-231 PGK eGFP luc spheroids with an initial seed count of 5,000 cells and addition of different Geltrex concentrationor collagen I. Read out was perfomed at different addition times. The RFU shown is the average of N=5 spheroids (one measurement per spheroid) and normalised to the first measurement (=D4). D=day.

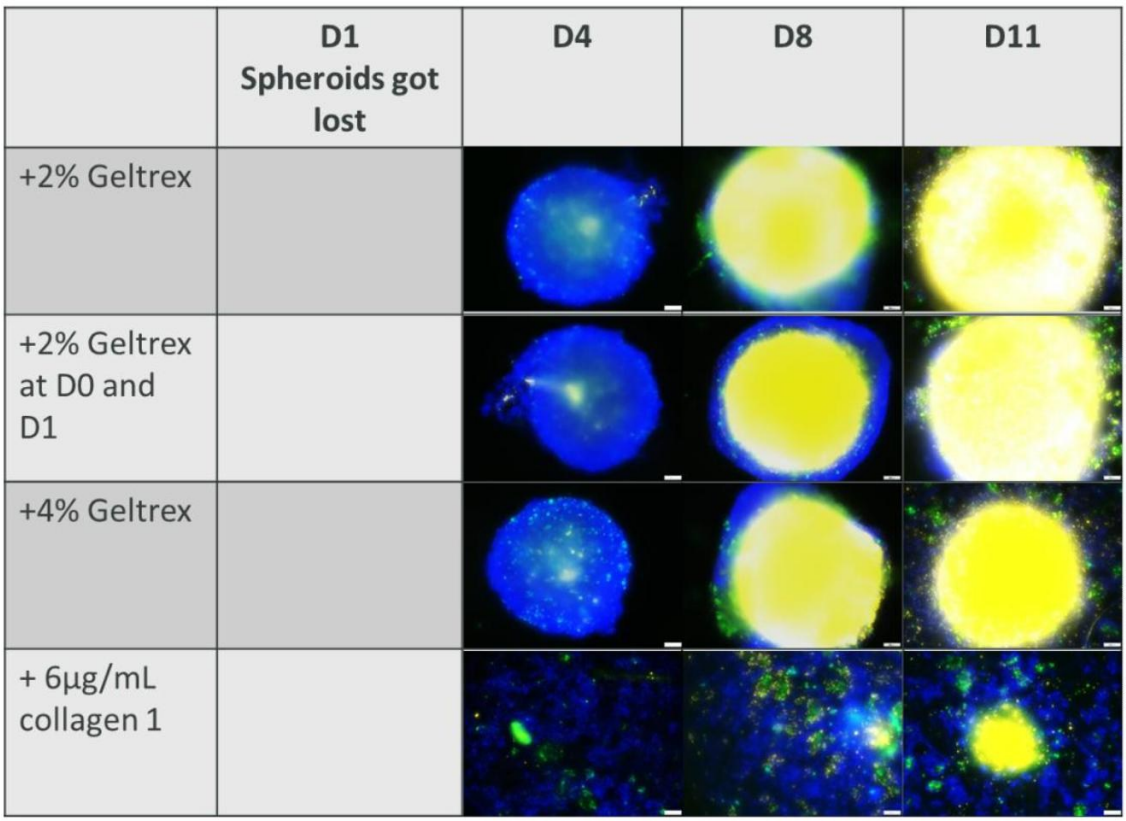

Figure 28: Necrotic core staining of 5,000 MDA-MB-231 PGK eGFP luc spheroids with collagen and different Geltrex concentrations via fluorescence microscopy (FLM). Spheroids were stained with Hoechst and PI (2 hours incubation time). Images were captured as Z-stacks (exposure time for Hoechst=20 ms with DAPI filter, conc. 16 µg/mL; exposure time for PI=10 ms with Cy3 filter, conc. 0.5 mg/mL; exposure time for the FITC filter =20 ms to see the eGFP labelled cells) and the maximum projection was extracted. The shown images show one out of n=3 spheroids. D=day. Scale bar = 100 µm.

Figure 29 shows the live-dead staining from the second experiment. It is interesting to note that the green signals (eGFP positive cells) have all gathered around the outside of the spheroid. Furthermore, the eGFP-labelled cells appear to have no nucleus (blue). Therefore, the signal could be caused by dead cells or some component in the matrix. Dead cells (yellow) are initially located around the compact core of the spheroid and near the labelled cells. From day 8 onwards, as in the first experiment, an accumulation of dead cells can be seen in the core of the spheroids, which continues to grow.

The spheroids used for live-dead staining were then harvested, cut and stained with both H/E for general evaluation of the morphology and for proliferative cells using anti KI-67 antibody and a FL-labelled secondary antibody.

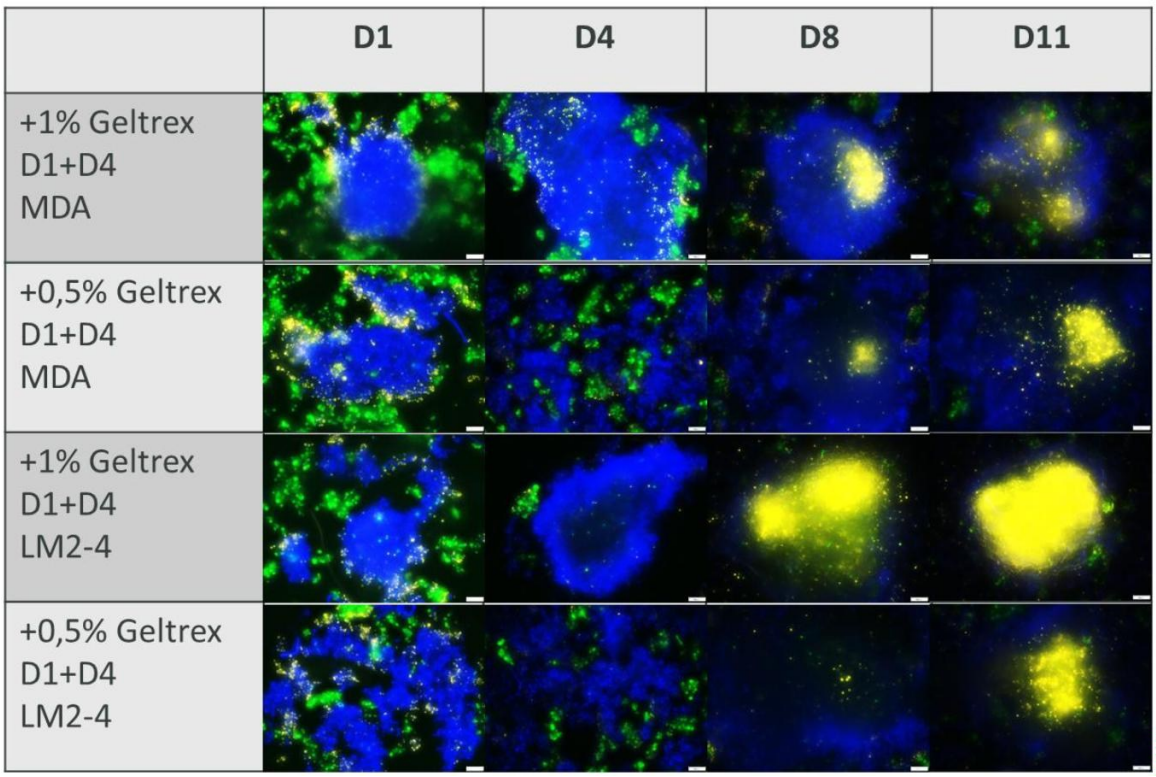

Figure 29: Necrotic core staining of 5,000 MDA-MB-231 PGK eGFP luc spheroids and MDA-MB-231 LM2-4 eGFP luc Spheroids with different Geltrex concentrations via fluorescence microscopy (FLM). Spheroids were stained with Hoechst and PI (2 hours incubation time). Images were captured as Z-stacks (exposure time for Hoechst=20 ms with DAPI filter, conc. 16 µg/mL; exposure time for PI=10 ms with Cy3 filter, conc. 0.5 mg/mL; exposure time for the FITC filter =20 ms to visualise the eGFP labelled cells) and the assumed maximum projection was extracted. The shown images show one out of n=3 spheroids. 2 h incubation time for the staining solutions; D=day.

Figure 30 shows a haematoxylin/eosin-stained section of MDA-MB-231 PGK eGFP luc and MDA-MB-231 LM2-4 eGFP luc from days 4 and 8. The spheroids are not stable

enough to withstand sectioning with the cryostat without damage. All cell nuclei are shown in blue, and the cytoplasm of the cells is stained pink.

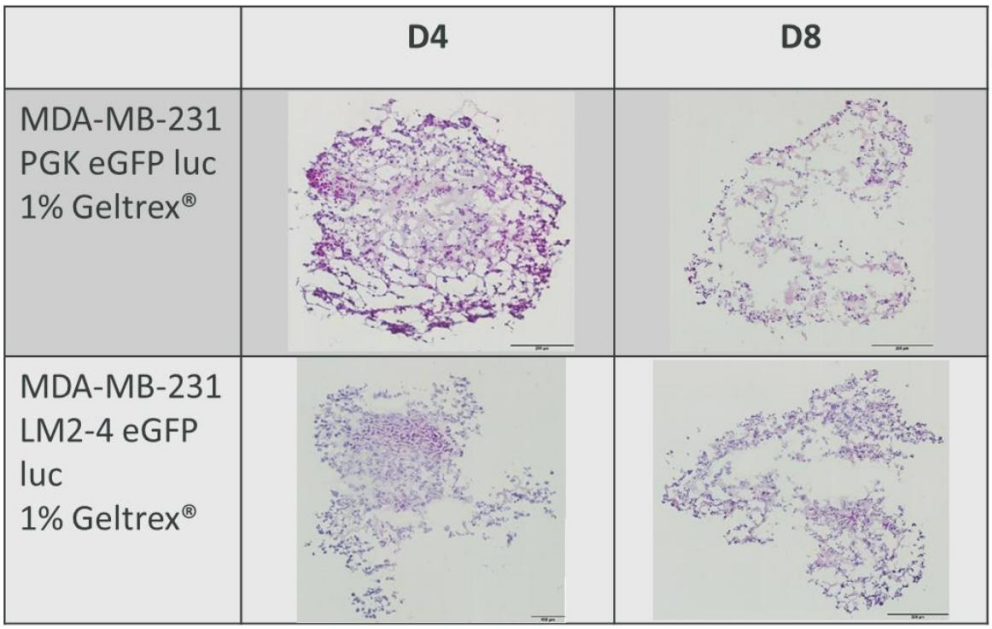

Figure 30: Photos of histological sections of MDA-MB-231 PGK eGFP luc and MDA-MB-231LM2-4 eGFP luc spheroids, each with 2x1% Geltrex, stained with haematoxylin and eosin on days 4 (=D4) and 8 (=D8). Scale bar= 100 µm.

Similarly, when stained with the anti Ki-67 antibody and FL-labelled secondary antibody, the spheroids did not remain compact (Figure 31). However, it can be observed that the different concentrations of the antibody show different signal intensities in the Ki-67 filter. Furthermore, since these are sections from day 4, there are hardly any dead cells visible in the PI filter. As with necrotic core staining, the DAPI filter shows all cell nuclei of the spheroids. The overlay of all filters clearly shows where exactly the secondary antibody has bound in the spheroid. Overall, high number of proliferative cells can be seen for both cell lines, but especially for MDA-MB-231 PGK eGFP luc. Interestingly, the proliferating cells can be found all over the surface of the spheroid section. This also fits to the result of the necrotic core staining, as at the earlier time point (D4) no pronounced necrotic core could be observed.

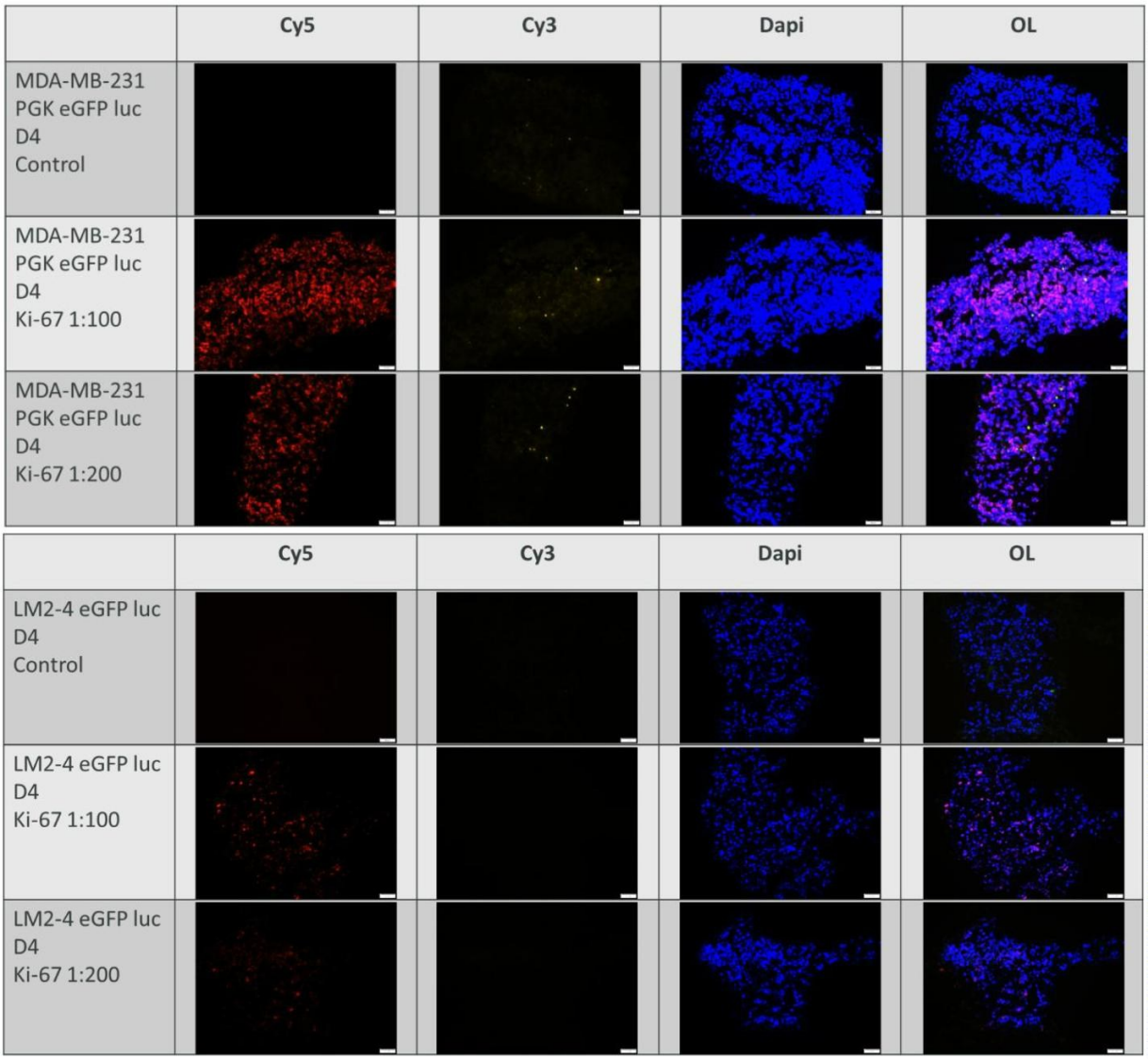

Figure 31:Images of sections stained with FL-labelled secondary antibodies from the cell lines MDA-MB-231 PGK eGFP luc and MDA-MB-231 LM2-4 eGFP luc, each with 2x 1% Geltrex on day 4. Ki-67 is shown with the Cy5 filter. The Cy3 filter shows the cells stained with PI (from the live-dead staining) and DAPI shows the cell nuclei. Scale bar: 50 µm.

8.2. Multicellular breast cancer spheroids

The aim of this experiment was to form multicellular spheroids of the cell lines MDA-MB-231 PGK eGFP luc or MDA-MB-231 LM2-4 eGFP luc with a human mammary fibroblast cell line to mimic TNBC in a 3D *in vitro* model. For this purpose, the cells were seeded into a plate according to the scheme shown in Figure 13. Phase contrast photos were taken on days 4, 7, 10, 12 and 14 to document cell growth and spheroid formation.

Figure 32 shows that HMF3S cells produce compact spheroids with both 2,500 and 5,000 cells. When combined with MDA-MB-231 PGK eGFP luc or MDA-MB-231 LM2-4 also reasonably compact spheroids are formed. However, these only last for about a week, as a corona around the spheroid can be seen from day 7 onwards. The compact core also becomes smaller from day 7 onwards, while the looser part surrounding the spheroid becomes larger.

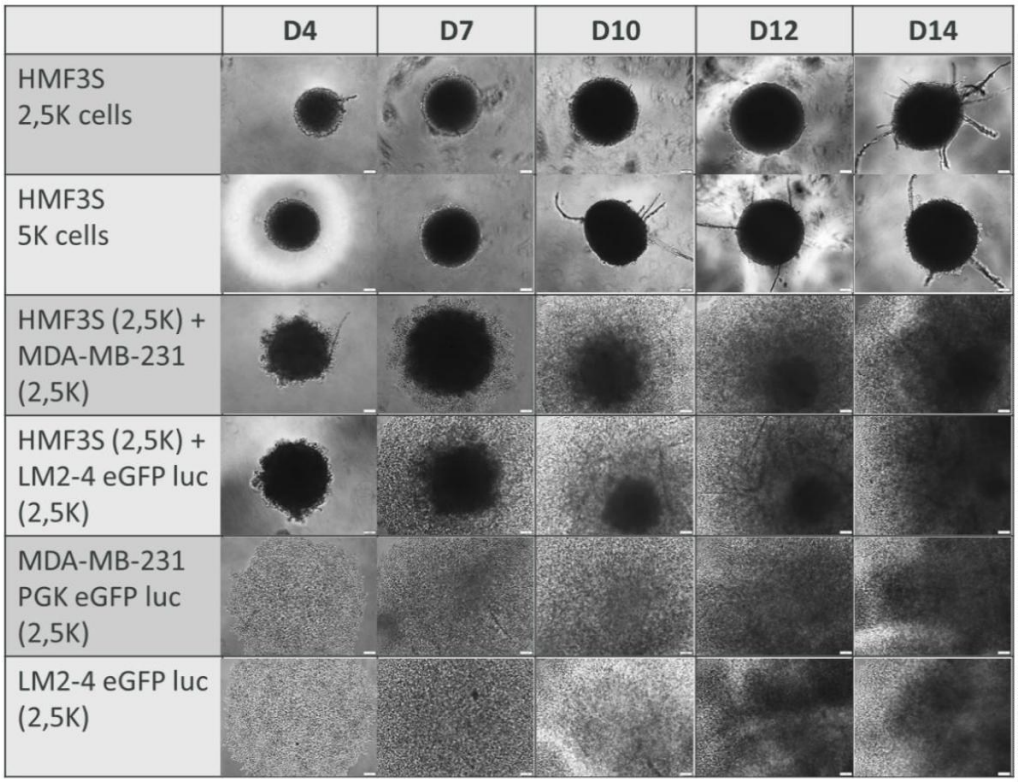

Figure 32: Phase contrast microscope images of HMF3S spheroids seeded with 2,500 (=2.5K) or 5,000 (=5K) cells, HMF3S with MDA-MB-231 PGK eGFP luc spheroids (2.5K and 2.5K) and HMF3S with MDA-MB-231 LM2-4 eGFP luc spheroids (2.5K and 2.5K). MDA-MB-231 PGK eGFP luc and MDA-MB-231 LM2-4 eGFP luc were seeded alone as a negative control (2,5K each). Pictures were taken at different growth times, according to the specified time points. One spheroid is shown as an example of n=5 spheroids. D=day; images were taken with exposure of 15 ms, 10x magnification, scale bar: 100µm

From day 4 onwards, a resazurin assay was also performed every other day to document cell growth.

Figure 33 shows that both the fibroblast mono-spheroids and the multicellular spheroids exhibit continuous growth. It is interesting to note that the two different

seeding counts of the fibroblast spheroids exhibit almost identical growth, which peaks on day 12, as the signal drops in all four by day 14.

In addition, live-dead staining was performed on days 4, 7, 10, 12 and 14 to see how many cells died over time and if a necrotic core is formed. Figure 34 shows that a small necrotic body can be found in the compact core of the spheroids as early as day 4. This necrotic core grows in the fibroblast mono-spheroids(HMF3S) over the entire period. The results are different for the multicellular spheroids, where only a small necrotic core can be seen on day 4, which increases further in a moderate way.. This indicates, that the monocellular spheroids are quite dense and form tight cell-cell connections, which hinders nutrients to penetrate into the inner part of the sphere. However, when combining them with the two TNBC cell lines, it seems that the construct gets less dense, but still enough cell-cell interactions are formed to result in a stable spheroid.

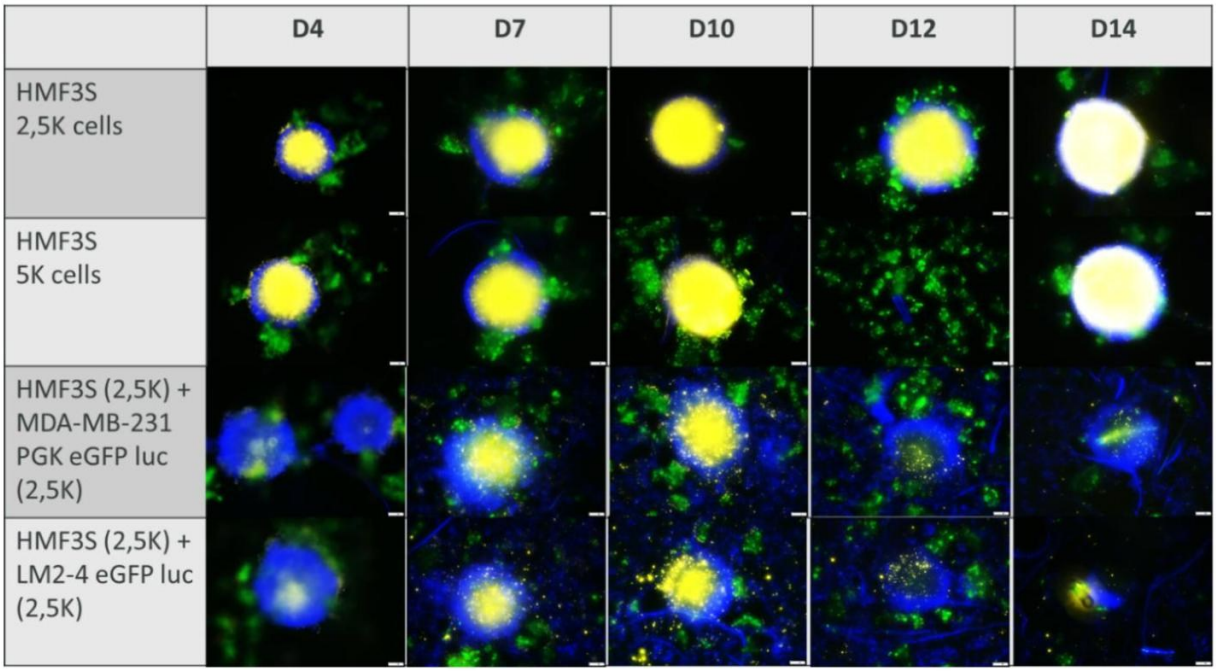

Figure 33: Necrotic core staining of spheroids seeded with 2,500 (=2.5K) or 5,000 (=5K) HMF3S cellsas well as multicellular spheroids with HMF3S (2,5K) and MDA-MB-231 PGK eGFP luc (2,5) or MDA-MB-231 LM2-4 eGFP luc (2.5).Spheroids were stained with Hoechst and PI (2 hours incubation time). Images were captured as Z-stacks (exposure time for Hoechst=20 ms with DAPI filter, conc. 16 µg/mL; exposure time for PI=10 ms with Cy3 filter, conc. 0,5 mg/mL; exposure time for the FITC filter =20 ms to visualise the eGFP labelled cells) and maximum projection image wasextracted. The shown images show one out of n=3 spheroids.D=day. Scale bar: 100 µm

With the mono-spheroids of the two cell lines, a similar strong necrotic core could only be shown with the addition of Geltrex®. This suggests, that those cells lines are not able to form sufficient cell-cell connections alone and need the help by either adding membrane matrix or co-cultivating them with fibroblasts. It is particularly interesting that although the fibroblasts are not labelled with eGFP, a green signal can be found. It is also interesting that the eGFP-labelled cells of the multicellular spheroids are mainly found outside the compact core. This indicates that either cells were transferred into the wrong wells accidentally or something in the media causes this strong fluorescent signal.

The spheroids used for live-dead staining were then harvested and stained with both H/E and FL-labelled secondary antibodies. Figure 35 shows the H/E-stained sections of the HMF3S and multicellular spheroids with additional MDA-MB-231 PGK eGFP luc or MDA-MB-231 LM2-4 eGFP luc. The fibroblasts have a major influence on the compactness of the multicellular spheroids. On their own, the HMF3S show a compact spheroid in both seeding counts of 2,500 K or 5,000 cells, which lasts for several days. The spheroids with HMF3S and MDA-MB-231 PGK eGFP luc are still very compact on day 4, but become looser again by day 7, although this could also be due to destruction by the section. The multicellular spheroids with MDA-MB-231 LM2-4 eGFP luc also have a compact structure. In both multicellular spheroids, it can be seen on day 7 that the cells on the outside are slightly larger than those on the inside, indicating that those are the tumour cells. However, the two cell types can not be distinguished with that staining and no clear structural organisation can be observed.

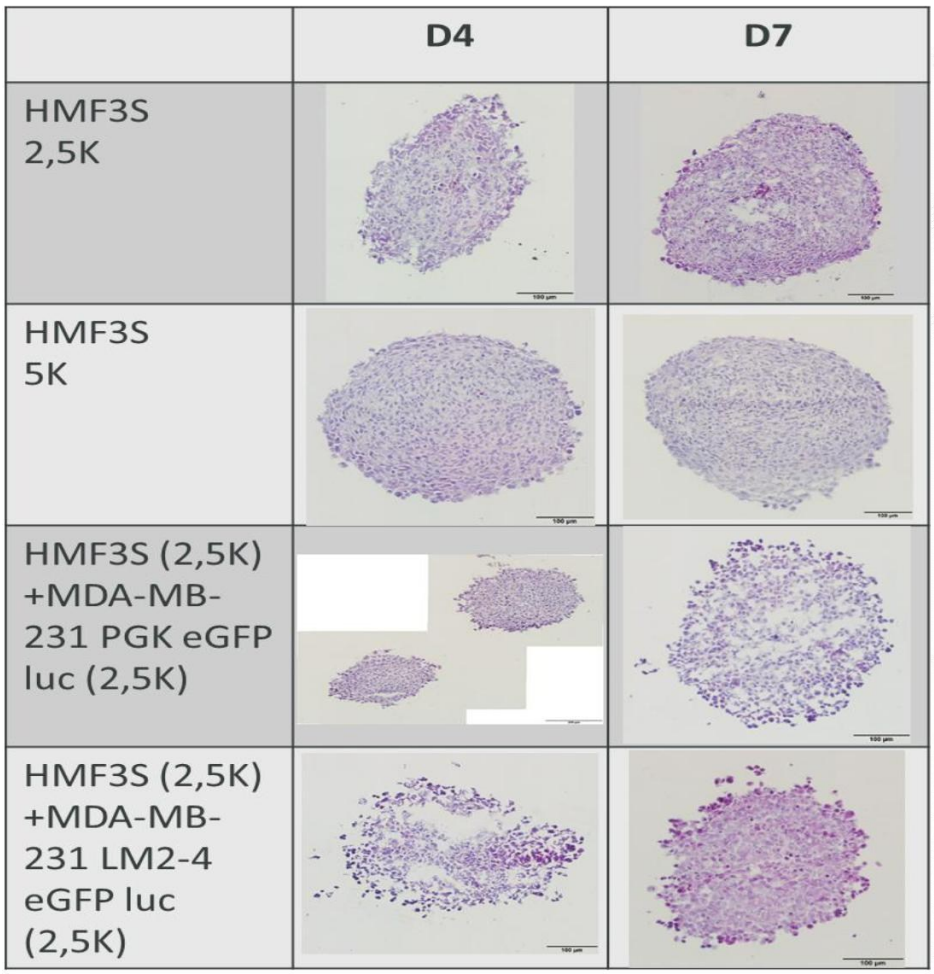

Figure 34: Photos of histological sections of HMF3S (2.5K and 5K) spheroids as well as multicellular spheroids with MDA-MB-231 PGK eGFP luc or MDA-MB-231LM2-4 eGFP luc, stained with haematoxylin and eosin on days 4 and 7. Scale bar: 100 µm

Figure 36 shows photos taken with a fluorescence microscope of 4 days old HMF3S spheroids with 2,500 or 5,000 cells seeded. The good density of the cell nuclei with DAPI is clearly visible. It is also clear to see that the different concentrations of KI-67 also produce signals of varying intensity in the spheroids. The location where the antibodies have bound is also clearly visible, as is the necrotic core inside the spheroid. Interestingly, proliferative cells can be detected across the section overlapping with the necrotic zone and not only on the outer rim.

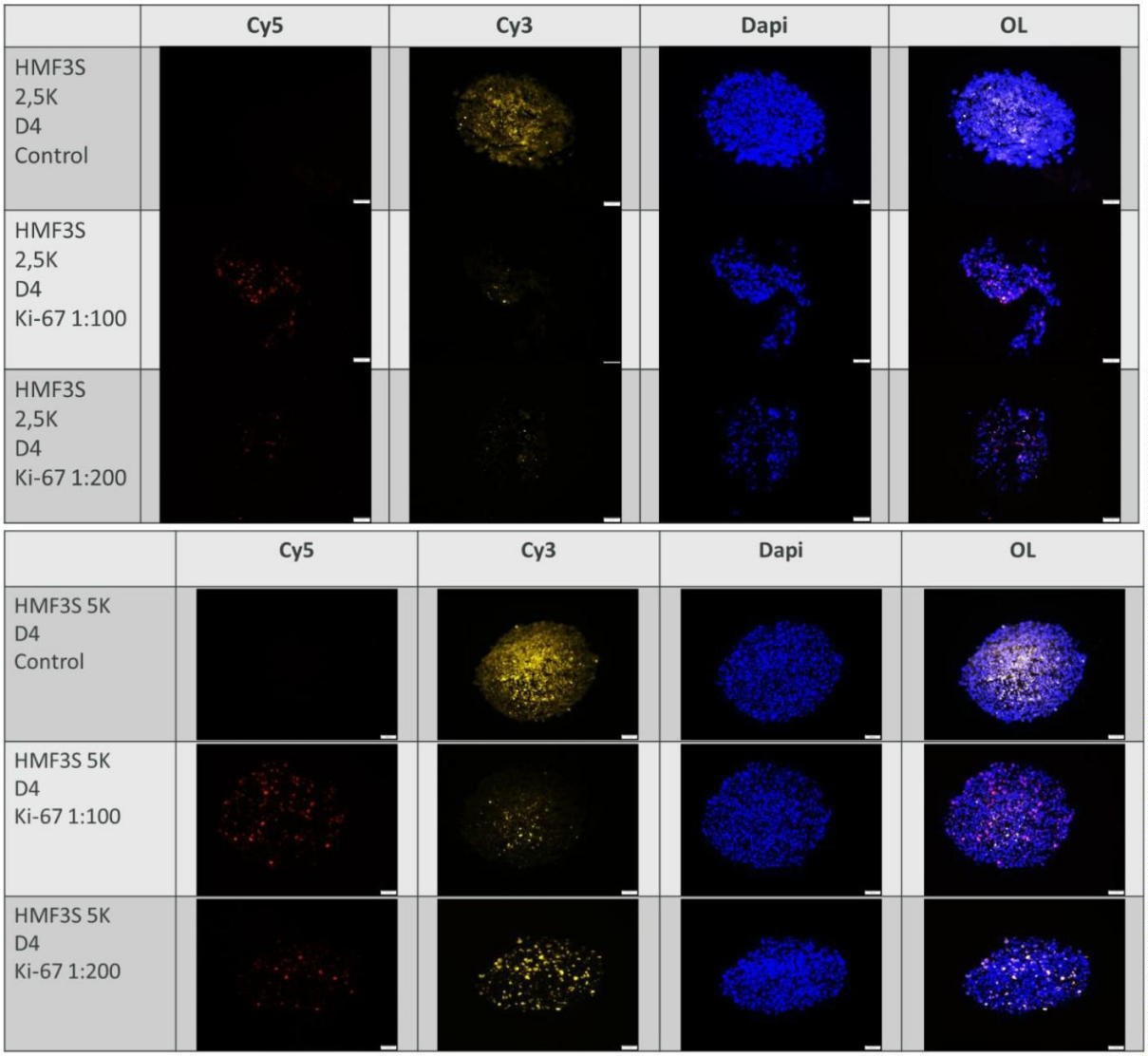

Figure 35: Images of sections stained with anti-Ki-67 antibody from the cell line HMF3S (2,500 = 2.5K and 5,000=5K cells seeded initially) on day 4. Ki-67 is shown with the Cy5 filter. The Cy3 filter shows the cells stained with PI and DAPI shows the cell nuclei. Scale bar: 50 µm

Figure 37 also shows photos from the IHC staining for proliferative cells of the multicellular spheroids taken with a fluorescence microscope. Above are the multicellular spheroids of HMF3S with MDA-MB-231 PGK eGFP luc cell lines, and below

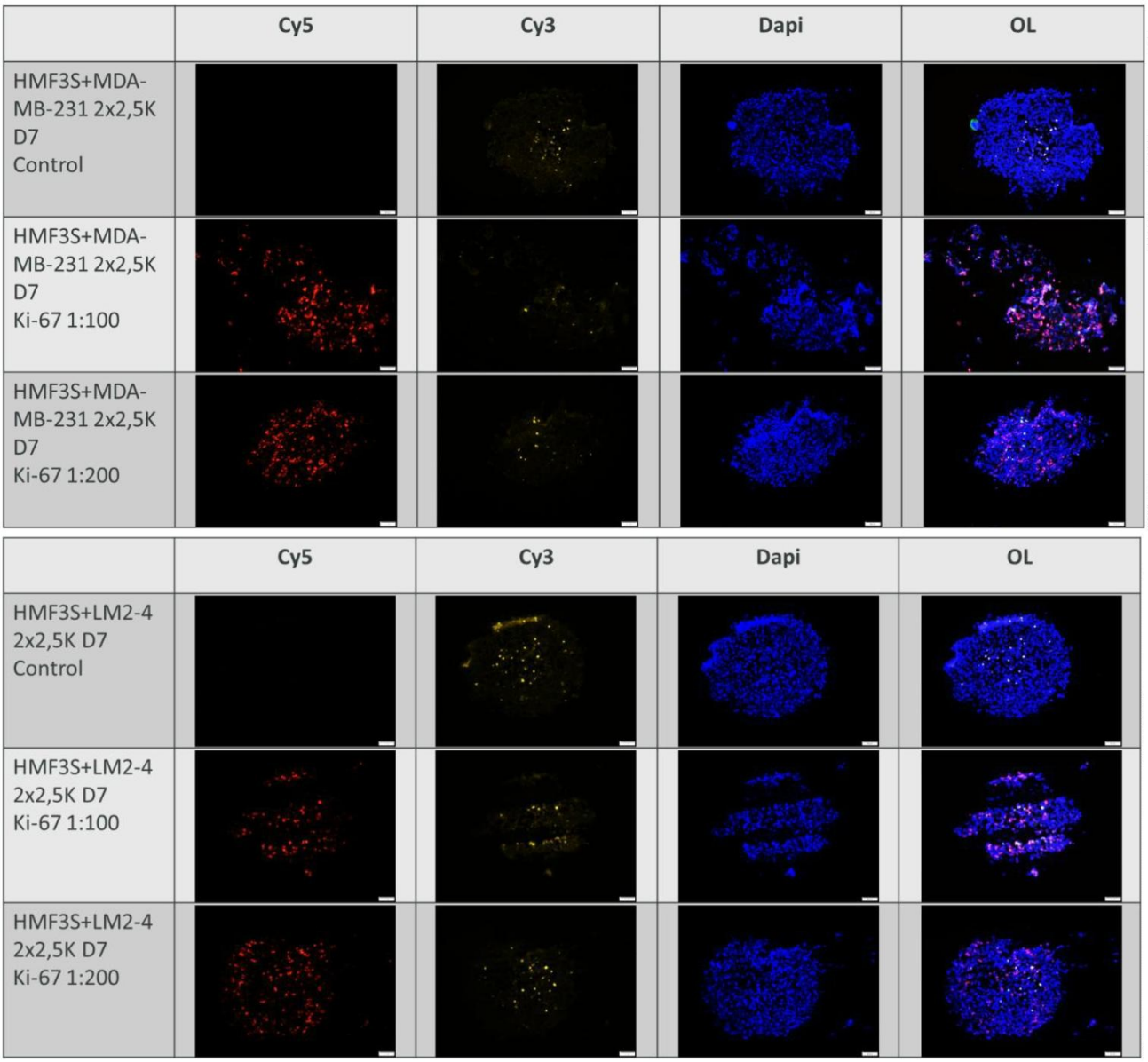

Figure 36: Images of sections stained with anti-Ki-67 antibody from the multicellular spheroids with HMF3S and MDA-MB-231 PGK eGFP luc (named as MDA-MB-231) or with MDA-MB-231 LM2-4 eGFP luc (named as LM2-4) on day 7 (initial seeding count 2,500 cells for each cell line = 2x2,5K). Ki-67 is shown with the Cy5 filter. The Cy3 filter shows the cells stained with PI and DAPI shows the cell nuclei. Scale bar: 50 µm

are the multicellular spheroids of HMF3S with MDA-MB-231 LM2-4 eGFP luc. The concentration-dependent staining of the Ki-67 antibody with the secondary antibody is clearly visible here, as well as the good density of the cell nuclei with DAPI. The signal for proliferative cells is stronger in intensity as well as in quantity when comparing it to the HMF3S mono-spheroids, which could be because both breast cancer cell lines prefer a loose cell structure. Unlike the HMF3S spheroids, the PI-stained cells are not located inside the core but are distributed throughout the spheroid, which may be because the dead cells in the breast cancer cells tend to occur in the eGFP-labelled cells, and these are distributed throughout the spheroid. Additionally, more cells are PI positive in the HMF3S monospheroids compared to when combined with the tumour cell lines, which aligns with the results from the necrotic core staining and live imaging.

9. CONCLUSION

Neither the MDA-MB-231 PGK eGFP luc cell line nor the MDA-MB-231 LM2-4 eGFP luc cell line formed spheroids on their own, although this was reported in various literature sources (67,68). The addition of collagen I alone did not result in the formation of spheroids, although Daniela Gruber's work ‘Optimisation of firefly luciferase assay in spheroid cell culture models’ was followed.

The addition of collagen I and subsequent centrifugation resulted in more compact cell aggregates, but these were too fragile to harvest. They also showed less cell death within the cell cluster during necrotic core staining. These cell aggregates could be used for all experiments that are only performed in the plate and require a small number of dying cells.

The addition of Geltrex resulted in compact spheroids that could also be harvested Howeverthey also showed a large necrotic core early on in the necrotic core staining. Therefore, this variant is a good option if the aim is to harvest spheroids and it does not matter if they form a large necrotic core.

Co-cultivation with the fibroblast cell line HMF3S shows an *in vitro* model that is very similar to the *in vivo* models. They showed compact spheroids up to day seven and a smaller necrotic core compared to the HMF3S mono-spheroids. The model needs to be further optimised to obtain compact spheroids for longer, especially regarding the ratio of the two cell types to come close to the actual tumour microenvironment.

Depending on the requirements of the experiment, the different variants of the MDA-MB-231 PGK eGFP luc and MDA-MB-231 LM2-4 eGFP luc cell lines can be used for cultivation, as they have different advantages and disadvantages.

Further optimisation steps must be carried out to obtain an ideal model of the MDA-MD-231 spheroids that can be harvested, does not have an excessively large necrotic core and nevertheless remains compact for a longer period of time.

10. APPENDIX

10.1.1.1. MDA-MB-231 PGK eGFP luc spheroids with different collagen concentrations and centrifugation

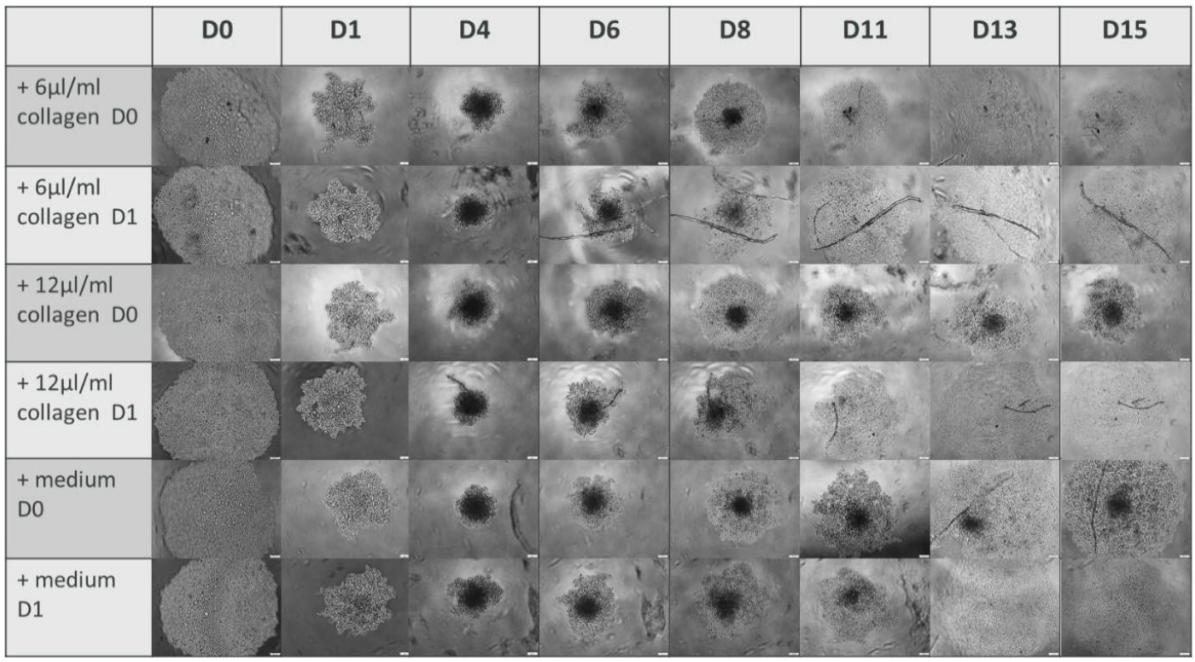

Figure 37: Phase contrast microscope images of MDA-MB-231 PGK eGFP luc spheroids from cell countof 5K (5K) at different growth times, according to the specified time points. One spheroid per collagen concentration (+ 6 µg/mL or 12 µg/mL collagen) or only medium (D0 and D1) is shown as an example n=5 spheroids. D=day; images with exposure of 15 ms, 10x magnification, scale bar: 100µm

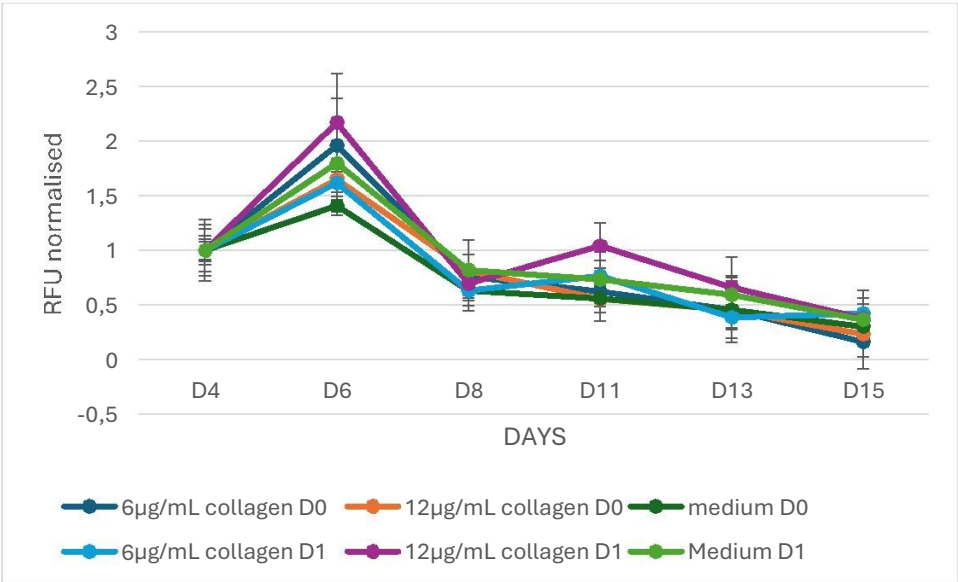

Figure 38: Average fluorescence signal (RFU) by resazurin cell viability assay of MDA-MB-231 PGK eGFP luc spheroids with an initial seed count of 5,000 (=5K) cells and different collagen concentration at different addition times. The RFU shown is the average of N=4 (only medium n=2) spheroids (one measurement per spheroid), normalised to the first measurement (=D4). D=day.

10.1.1.2. MDA-MB-231 PGK eGFP luc spheroids with basement membrane matrix

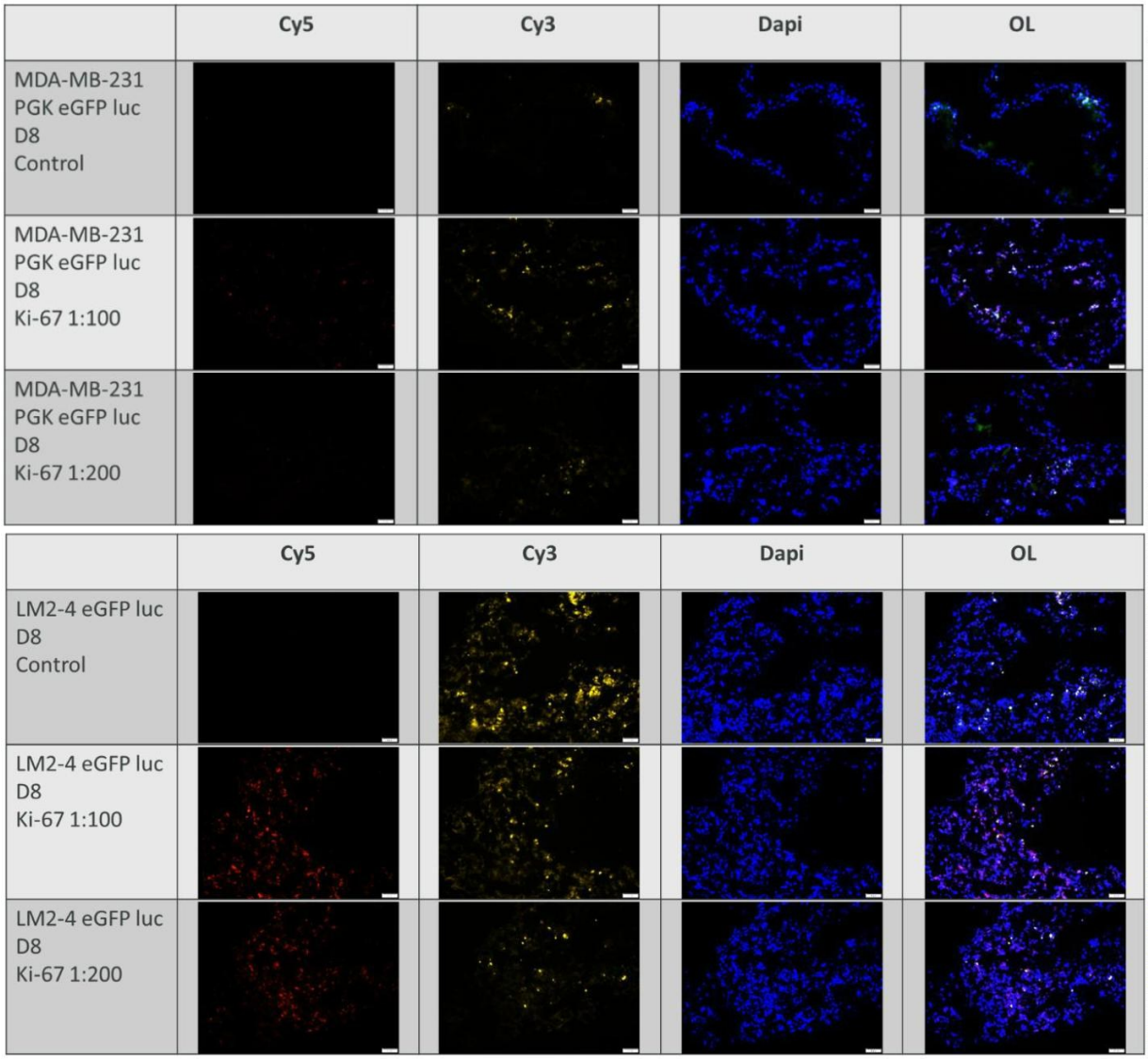

Figure 39: Images of sections stained with FL-labelled secondary antibodies from the cell lines MDA-MB-231 PGK eGFP luc and MDA-MB-231 LM2-4 eGFP luc, each with 2x 1% Geltrex on day 4. Ki-67 is shown with the Cy5 filter. The Cy3 filter shows the cells stained with PI and Dapi shows the cell nuclei. Scale bar: 50 µm.

10.2. Multicellular breast cancer spheroids

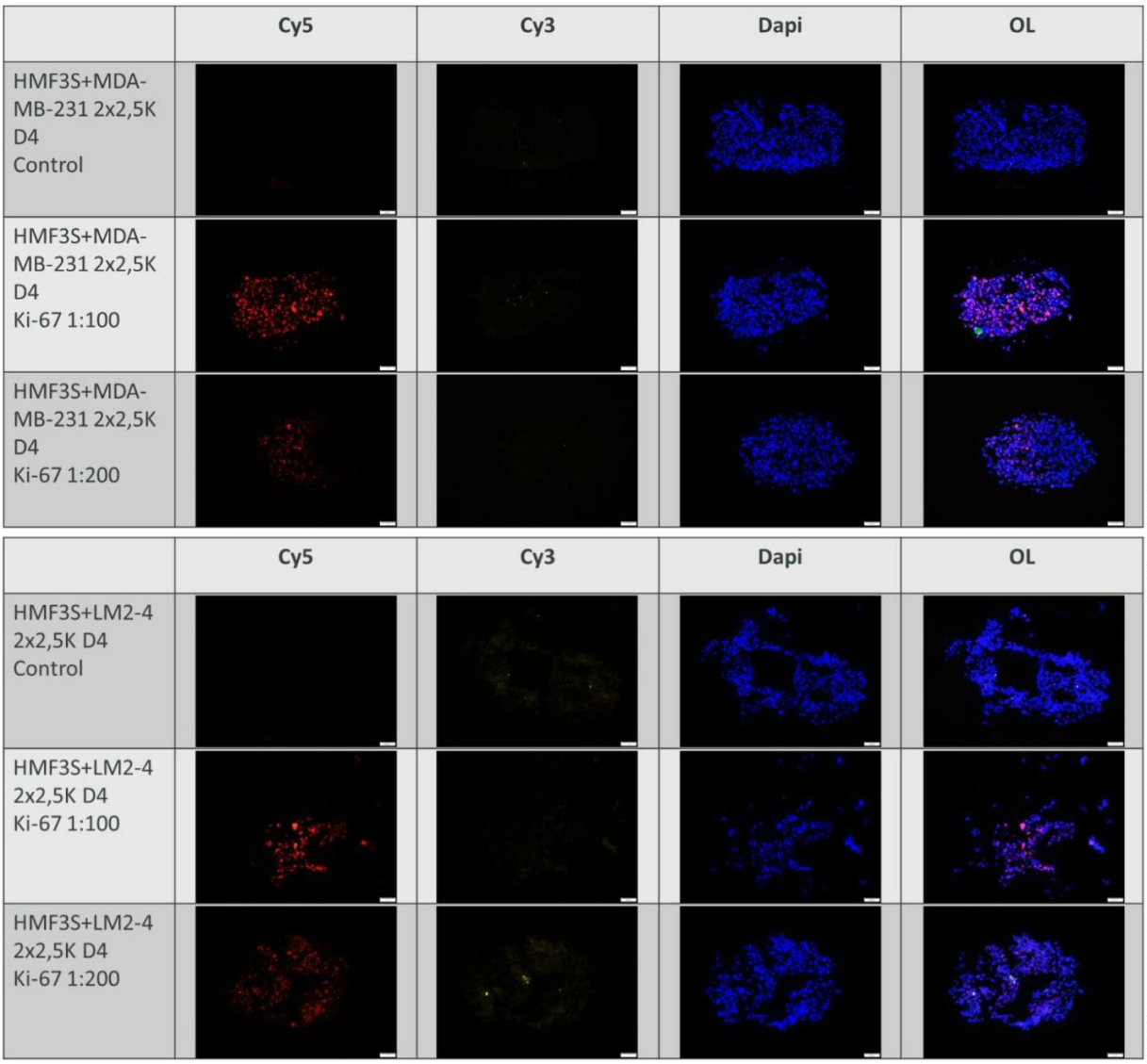

Figure 40: Images of sections stained with FL-labelled secondary antibodies from D4 multicellular spheroids with HMF3S and MDA-MB-231 PGK eGFP luc (named as MDA-MB-231) or with MDA-MB-231 LM2-4 eGFP luc (named as LM2-4) seeded 2,500 cells each (=2y2,5K). Ki-67 is shown with the Cy5 filter. The Cy3 filter shows the cells stained with PI and Dapi shows the cell nuclei. Scale bar: 50 µm.

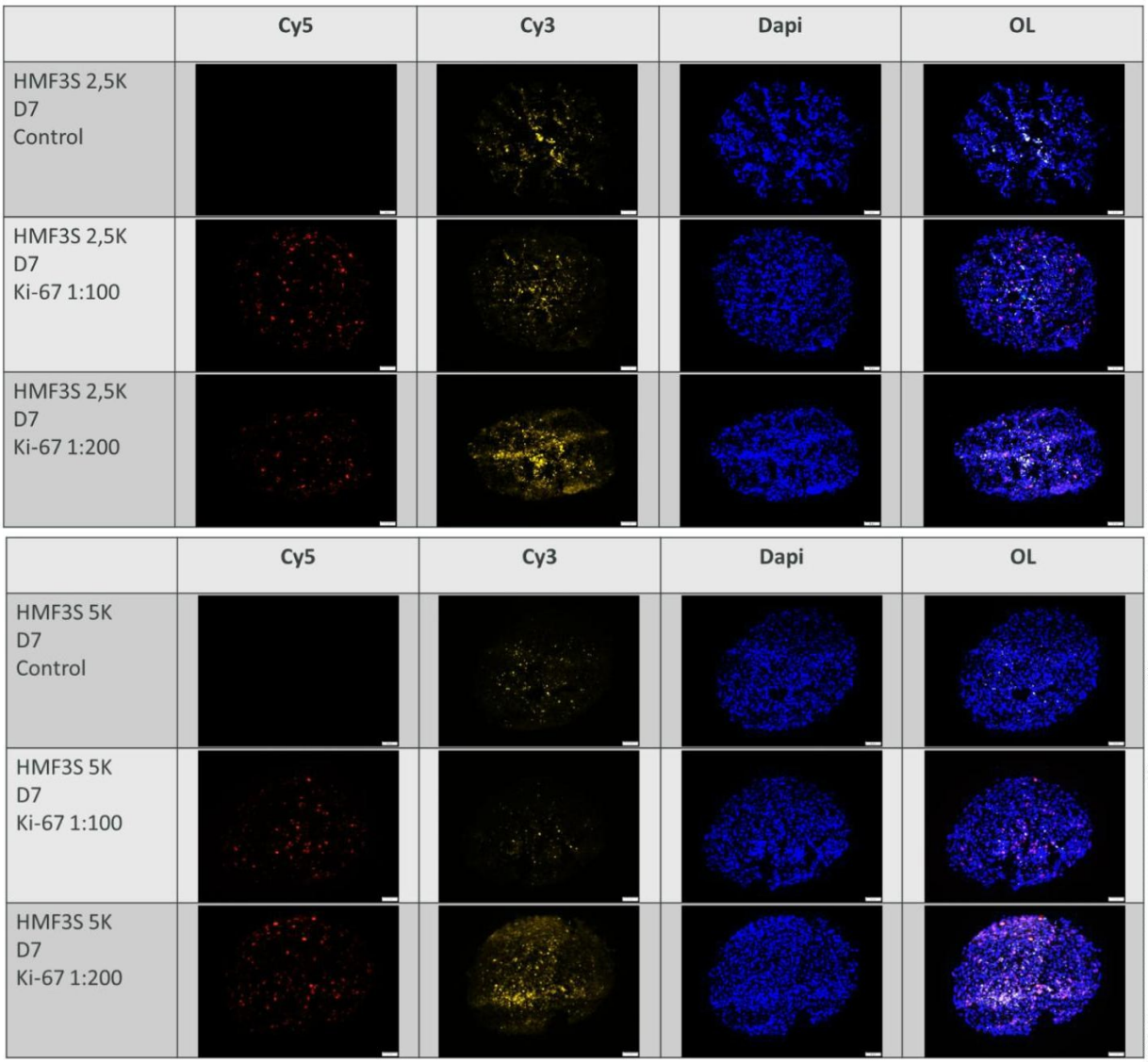

Figure 41: Images of sections stained with FL-labelled secondary antibodies from D4 spheroids ofthe cell line HMF3S seeded with 2,500 (=2.5K) or 5,000 (=5K) cells. Ki-67 is shown with the Cy5 filter. The Cy3 filter shows the cells stained with PI and Dapi shows the cell nuclei. Scale bar: 50 µm.

11. LIST OF FIGURES

12. REFERENCES

1. Trishna S, Solomon J, Samson AO, Gil-Henn H. Invasion and Metastasis as a Central Hallmark of Breast Cancer [Internet]. MDPI; 2021. Available from: https://doi.org/10.3390/jcm10163498

2. Xiaofeng D, Liangjian X, Ting L, Zhonghu B. Cancer Hallmarks, Biomarkers and Breast Cancer Molecular Subtypes [Internet]. Ivyspring International Publisher; 2016. Available from: doi:10.7150/jca.13141

3. Sung H, Ferlay J, Siegel RL, Laversanne M, Soerjomataram I, Jemal A, et al. Global Cancer Statistics 2020: GLOBOCAN Estimates of Incidence and Mortality Worldwide for 36 Cancers in 185 Countries [Internet]. Cancer Journal; 2021. Available from: doi: 10.3322/caac.21660.

4. Polyak K. Heterogeneity in breast cancer [Internet]. The Journal of Clinical Investigation; 2011. Available from: doi:10.1172/JCI60534

5. Lopez-Gonzalez L, Sanchez Cendra A, Sanchez Cendra C, Roberts Cervantes ED, Cassinello Espinosa J, Pekarek T, et al. Exploring Biomarkers in Breast Cancer: Hallmarks of Diagnosis, Treatment, and Follow-Up in Clinical Practice [Internet]. MDPI; 2024. Available from: https://doi.org/10.3390/medicina60010168

6. Turner KM, Yeo SK, Holm TM, Shaughnessy E, Guan JL. Heterogeneity within molecular subtypes of breast cancer [Internet]. American Journal of Physiology - Cell Physiology; 2021. Available from: doi:10.1152/ajpcell.00109.2021

7. Prat A, Perou CM. Deconstructing the molecular portraits of breast cancer [Internet]. ScienceDirect; 2010. Available from: doi:10.1016/j.molonc.2010.11.003

8. Bianchini G, Balko JM, Mayer IA, Sanders ME, Gianni L. Triple-negative breast cancer: challenges and opportunities of a heterogeneous disease [Internet]. Nat Rev Clin Oncol.; 2016. Available from: doi:10.1038/nrclinonc.2016.66

9. Kaur P, Nagaraja GM, Zheng H, Gizachew D, Galukande M, Krishnan S, et al. A mouse model for triple-negative breast cancer tumor-initiating cells (TNBC-TICs) exhibits similar aggressive phenotype to the human disease [Internet]. BMC Cancer; 2012. Available from: https://doi.org/10.1186/1471-2407-12-120.

10. Hanahan D. Hallmarks of Cancer: New Dimensions [Internet]. American Association for Cancer Research; 2022. Available from: doi: 10.1158/2159-8290.CD-21-1059

11. Hanahan D, Weinberg RA. Hallmarks of Cancer: The Next Generation [Internet]. Cell; 2011. Available from: doi:10.1016/j.cell.2011.02.013

12. Castellanos G, Valbuena DS, Perez E, Villegas VE, Rondon-Lagos M. Chromosomal Instability as Enabling Feature and Central Hallmark of Breast Cancer [Internet]. Breast Cancer (Dove Med Press); 2023. Available from: doi:10.2147/BCTT.S383759

13. Linet MS, Slovis TL, Miller DL, Kleinerman R, Lee C, Rajaraman P, et al. Cancer Risks Associated with External Radiation From Diagnostic Imaging Procedures [Internet]. CA Cancer J Clin.; 2012. Available from: doi:10.3322/caac.21132.

14. De Guzman R, Schiller J. Air pollution and its impact on cancer incidence, cancer care and cancer outcomes [Internet]. BMJ Oncol.; 2025. Available from: dio:10.1136/bmjonc-2024-000535

15. National Institute of Environmental Health Sciences [Internet]. 06/25. Breast Cancer. Available from: https://www.niehs.nih.gov/health/topics/conditions/breast-cancer

16. Gearhart-Serna LM, Mills BA, Hsu H, Fayanju OM, Hoffman K, Devi GR. Cumulative environmental quality is associated with breast cancer incidence differentially by summary stage and urbanicity [Internet]. Scientific Reports; 2023. Available from: doi:20301

17. La Merrill MA, Vandenberg LN, Smith MT, Goodson W, Browne P, Patisaul HB, et al. Consensus on the key characteristics of endocrine-disrupting chemicals as a basis for hazard identification [Internet]. Nat Rev Endocrinol.; 2019. Available from: doi: 10.1038/s41574-019-0273-8

18. Green Brody J, Moysich KB, Humblet O, Attfield KR, Beehler GP, Rudel RA. Environmental Pollutants and Breast Cancer: Epidemiologic studies [Internet]. Wiley InterScience; 2007. Available from: doi:10.1002/cncr.22655

19. DeRoo LA, Cummings P, Mueller BA. Smoking Before the First Pregnancy and the Risk of Breast Cancer: A Meta-Analysis [Internet]. American Journal of Epidemiology; 2011. Available from: doi: 10.1093/aje/kwr090

20. Scoccianti C, Cecchini M, Anderson AS, Berrino F, Boutron-Ruault MC, Espina C, et al. European Code against Cancer 4th Edition: Alcohol drinking and cancer [Internet]. Cancer Epidemiology; 2016. Available from: https://doi.org/10.1016/j.canep.2016.09.011

21. Manouchehri E, Taghipour A, Ghavami V, Ebadi A, Homaei F, Latifnejad Roudsari R. Night-shift work duration and breast cancer risk: an updated systematic review and meta-analysis [Internet]. BMC Women's Health; 2021. Available from: doi:10.1186/s12905-021-01233-4

22. Wolff MS, Weston A. Breast Cancer Risk and Environmental Exposures [Internet]. Environmental Health Perspectives; 1997. Available from: doi:10.1289/ehp.97105s4891

23. National Breast Cancer Foundation,INC. [Internet]. 06/25. Risk Factors. Available from: ctive smoking and breast cancer risk: original cohort data and meta-analysis.

24. Quail DF, Joyce JA. Microenvironmental regulation of tumor progression and metastasis [Internet]. Nat Med. Author manuscript; 2013. Available from: doi: 10.1038/nm.3394

25. Xiong X, Zheng LW, Ding Y, Cai YW, Wang LP, Huang L, et al. Breast cancer: pathogenesis and treatments [Internet]. Signal Transduction and Targeted Therapy; 2025. Available from: https://doi.org/10.1038/s41392-024-02108-4

26. Moura T, Laranjeira P, Caramelo O, Gil AM, Paiva A. Breast Cancer and Tumor Microenvironment: The Crucial Role of Immune Cells [Internet]. Current Oncology; 2025. Available from: doi: 10.3390/curroncol32030143

27. Li JJ, Tsang JY, Tse GM. Tumor Microenvironment in Breast Cancer—Updates on Therapeutic Implications and Pathologic Assessment [Internet]. Cancers; 2021. Available from: doi: 10.3390/cancers13164233

28. Place AE, Polyak K, Jin Huh S. The microenvironment in breast cancer progression: biology and implications for treatment [Internet]. Breast Cancer Research; 2011. Available from: https://doi.org/10.1186/bcr2912

29. Niland S, Riscanevo AX, Eble JA. Matrix Metalloproteinases Shape the Tumor Microenvironment in Cancer Progression [Internet]. International Journal of Molecular Science; 2021. Available from: doi: 10.3390/ijms23010146

30. Binnewies M, Roberts EW, Kersten K, Chan V, Fearon DF, Merad M, et al. Understanding the tumor immune microenvironment (TIME) for effective therapy [Internet]. Nat. Med; 2018. Available from: doi: 10.1038/s41591-018-0014-x

31. Fan Y, He S. The Characteristics of Tumor Microenvironment in Triple Negative Breast Cancer [Internet]. Cancer Management and Research; 2022. Available from: doi: 10.2147/CMAR.S316700

32. Ruffell B, Coussens LM. Macropahes and therapeutic resistace in cancer [Internet]. Cancer Cell; 2015. Available from: doi: 10.1016/j.ccell.2015.02.015

33. Zannetti A. Breast Cancer: From Pathophysiology to Novel Therapeutic Approaches 2.0 [Internet]. International Journal of Molecular Science; 2023. Available from: doi: 10.3390/ijms24032542

34. Kan JY, Lee HC, Hou MF, Tsai HP, Chang CY, Tsai PH, et al. Metabolic shifts in lipid utilization and reciprocal interactions within the lung metastatic niche of triple-negative breast cancer revealed by spatial multi-omics [Internet]. Cell Death & Disease; 2024. Available from: https://doi.org/10.1038/s41419-024-07205-4

35. Wang J, Zhao H, Ye L, Li J, Zhang H, Zhang C, et al. Diagnostic and Prognostic Nomograms for Lung Metastasis in Triple-Negative Breast Cancer [Internet]. Comput Math Methods Med; 2022. Available from: doi: 10.1155/2022/1750834

36. Khan SU, Xia Y, Goodale D, Schoettle G, Allan AL. Lung-Derived Selectins Enhance Metastatic Behavior of TripleNegative Breast Cancer Cells [Internet]. Biomedicines; 2021. Available from: doi: 10.3390/biomedicines9111580

37. Minn AJ, Gupta GP, Padua D, Bos P, Nguyen DX, Nuyten D, et al. Lung metastasis genes couple breast tumor size and metastatic spread [Internet]. Proc Natl Acad Sci U S A; 2007. Available from: doi: 10.1073/pnas.0701138104

38. Chue BMF, La Course BD. Case report of long-term survival with metastatic triple-negative breast carcinoma - Treatment possibilities for metastatic disease [Internet]. Medicine; 2019. Available from: DOI: 10.1097/MD.0000000000015302

39. Dupuy F, Tabaries S, Andrzejewski S, Dong Z, Blagih J, Annis MG, et al. PDK1-Dependent Metabolic Reprogramming Dictates Metastatic Potential in Breast Cancer [Internet]. Cell Metabolism; 2015. Available from: doi:10.1016/j.cmet.2015.08.007

40. Holliday DL, Speirs V. Choosing the right cell line for breast cancer research [Internet]. Breast Cancer Research; 2011. Available from: doi:10.1186/bcr2889

41. Koedoot E, Fokkelman M, Rogkoti VM, Smid M, van de Sandt I, de Bont H, et al. Uncovering the signaling landscape controlling breast cancer cell migration identifies novel metastasis driver genes [Internet]. Nature Communications; 2019. Available from: https://doi.org/10.1038/s41467-019-11020-3

42. Guerin E, Man S, Xu P, Kerbel RS. A MODEL OF POSTSURGICAL ADVANCED METASTATIC BREAST CANCER MORE ACCURATELY REPLICATES THE CLINICAL EFFICACY OF ANTIANGIOGENIC DRUGS [Internet]. Cancer Research; 2013. Available from: doi:10.1158/0008-5472.CAN-12-4183

43. Sun Q, Wang Y, Officer A, Pecknold B, Lee G, Harismendy O, et al. Stem-like breast cancer cells in the activated state resist genetic stress via TGFBI-ZEB1 [Internet]. npj Breast Cancer; 2022. Available from: https://doi.org/10.1038/s41523-021-00375-w

44. Kim MY, Oskarsson T, Acharyya S, Nguyen DX, Zhang XHF, Norton L, et al. Tumor Self-Seeding by Circulating Cancer Cells [Internet]. Cell; 2009. Available from: https://doi.org/10.1016/j.cell.2009.11.025

45. Maiti A, Takabe K, Hait NC. Metastatic triple-negative breast cancer is dependent on SphKs/S1P signaling for growth and survival [Internet]. Cell Signal; 2017. Available from: doi:10.1016/j.cellsig.2017.01.021

46. Munoz R, Man S, Shaked Y, Lee CR, Wong J, Francia G, et al. Highly efficacious nontoxic preclinical treatment for advanced metastatic breast cancer using combination oral UFT-cyclophosphamide metronomic chemotherapy [Internet]. Cancer Research; Available from: DOI: 10.1158/0008-5472.CAN-05-4411

47. Cook MT, Liang Y, Besch-Williford C, Hyder SM. Luteolin inhibits lung metastasis, cell migration, and viability of triple-negative breast cancer cells [Internet]. Dovepress; 2016. Available from: https://doi.org/10.2147/BCTT.S124860

48. Billerhart M, Schönhofer M, Schueffl H, Polzer W, Pichler J, Decker S, et al. CD47-targeted cancer immunogene therapy: Secreted SIRPα-Fc fusion protein eradicates tumors by macrophage and NK cell activation [Internet]. Molecular Therapie Oncolytics; 2021. Available from: DOI: 10.1016/j.omto.2021.09.005

49. Foglietta F, Canaparo R, Muccioli G, Terreno E, Serpe L. Methodological aspects and pharmacological applications of three-dimensional cancer cell cultures and organoids [Internet]. Life Sciences; 2020. Available from: https://doi.org/10.1016/j.lfs.2020.117784

50. Kapałczyńska M, Kolenda T, Przybyła W, Zajaczkowska M, Teresiak A, Filas V, et al. 2D and 3D cell cultures – a comparison of different types of cancer cell cultures [Internet]. Archives of Medical Science; 2016. Available from: doi:10.5114/aoms.2016.63743

51. Imamura Y, Mukohara T, Shimono Y, Funakoshi Y, Chayahara N, Toyoda M, et al. Comparison of 2D- and 3D-culture models as drug-testing platforms in breast cancer [Internet]. Oncology Reports; 2015. Available from: https://doi.org/10.3892/or.2015.3767

52. Breslin S, O'Driscoll L. The relevance of using 3D cell cultures, in addition to 2D monolayer cultures, when evaluating breast cancer drug sensitivity and resistance [Internet]. Oncotarget; 2016. Available from: doi:10.18632/oncotarget.9935

53. Cui X, Hartanto Y, Zhang H. Advances in multicellular spheroids formation [Internet]. J R Soc Interface; 2017. Available from: doi: 10.1098/rsif.2016.0877

54. Pinto B, Henriques AC, Silva PMA, Bousbaa H. Three-Dimensional Spheroids as In Vitro Preclinical Models for Cancer Research [Internet]. Pharmaceutics; 2022. Available from: doi: 10.3390/pharmaceutics12121186

55. Li Z, Cui Z. Three-dimensional perfused cell culture [Internet]. ScienceDirect; Available from: https://doi.org/10.1016/j.biotechadv.2013.10.006

56. Shen H, Cai S, Wu C, Yang W, Yu H, Liu L. Recent Advances in Three-Dimensional Multicellular Spheroid Culture and Future Development [Internet]. Micromachines; 2021. Available from: https://doi.org/10.3390/mi12010096

57. Singh S, Tran S, Putman J, Tavana H. Three-dimensional models of breast cancer–fibroblasts interactions [Internet]. Experimental Biology and Medicine; 2022. Available from: doi: 10.1177/1535370220917366

58. Yakavets I, Francois A, Benoit A, Merlin JL, Bezdetnaya L, Vogin G. Advanced co-culture 3D breast cancer model for investigation of fibrosis induced by external stimuli: optimization study [Internet]. Scientific Reports; 2020. Available from: https://doi.org/10.1038/s41598-020-78087-7

59. Domingues M, Pereira CL, Sarmento B, Castro F. Mimicking 3D breast tumor-stromal interactions to screen novel cancer therapeutics [Internet]. European Journal of

Pharmaceutical Sciences; 2023. Available from: https://doi.org/10.1016/j.ejps.2023.106560

60. Dang TT, Prechtl AM, Pearson GW. Breast Cancer Subtype-Specific Interactions with the Microenvironment Dictate Mechanisms of Invasion [Internet]. Cancer Research; 2011. Available from: https://doi.org/10.1158/0008-5472.CAN-11-1818

61. Osuala KO, Heyza J, Zhao Z, Xu Y, Moin K, Ji K, et al. Carcinoma-Associated Fibroblasts Accelerate Growth and Invasiveness of Breast Cancer Cells in 3D Long-Term Breast Cancer Models [Internet]. Cancers; 2024. Available from: https://doi.org/10.3390/cancers16223840

62. Li L, Lu Y. Optimizing a 3D Culture System to Study the Interaction between Epithelial Breast Cancer and Its Surrounding Fibroblasts [Internet]. Journal of Cancer; 2011. Available from: doi:10.7150/jca.2.458

63. Sadras F, Stewart TA, Robitaille M, Peters AA, Kalita-de Croft P, Soon PS, et al. Altered Calcium Influx Pathways in Cancer-Associated Fibroblasts [Internet]. Biomedicines; 2021. Available from: doi: 10.3390/biomedicines9060680

64. Olson CJ, Moreira J, Lukanidin EM, Ambartsumian NS. Human mammary fibroblasts stimulate invasion of breast cancer cells in a three-dimensional culture and increase stroma development in mouse xenografts [Internet]. BMC Cancer; 2010. Available from: doi: 10.1186/1471-2407-10-444

65. O'Hare MJ, Bond J, Clarke C, Takeuchi Y, Atherton AJ, Berry C, et al. Conditional immortalization of freshly isolated human mammary fibroblasts and endothelial cells. PNAS; 2001.

66. Wang K, Xie S, Xia H, Zhang X, He J. Establishment of a bioluminescent MDA-MB-231 cell line for human triple-negative breast cancer research [Internet]. Oncology Reports; 2012. Available from: DOI: 10.3892/or.2012.1742

67. Huang Z, Yu P, Tang J. Characterization of Triple-Negative Breast Cancer MDA-MB-231 Cell Spheroid Model [Internet]. OncoTargets and Therapy; 2020. Available from: doi: 10.2147/OTT.S249756

68. Ivascu A, Kubbies M. Rapid Generation of Single-Tumor Spheroids for High-Throughput Cell Function and Toxicity Analysis [Internet]. Journal of Biomolecular Screening; 2006. Available from: DOI:10.1177/1087057106292763

69. ThermoFisher SCIENTIFIC [Internet]. MDA-MB-231 Cell Line Spheroid Generation and Characterization for HT Assays. Available from: https://www.thermofisher.com/at/en/home/references/protocols/cell-culture/3-d-cell-culture-protocol/mda-mb-231-cell-line-spheroid-generation.html

70. Dubois C, Dufour R, Daumar P, Aubel C, Szczepaniak C, Blavignac C, et al. Development and cytotoxic response of two proliferative MDA-MB-231 and non-proliferative SUM1315 three-dimensional cell culture models of triple-negative

basal-like breast cancer cell lines [Internet]. Oncotarget; 2017. Available from: doi: 10.18632/oncotarget.20517

71. ThermoFisher SCIENTIFIC [Internet]. 2025. Geltrex Flex Basement Membrane Matrices. Available from: https://www.thermofisher.com/at/en/home/life-science/cell-culture/organoids-spheroids-3d-cell-culture/extracellular-matrices-ecm/geltrex-matrix-products.html